Ore Geology Reviews 86 (2017) 100–116

Contents lists available at ScienceDirect

Ore Geology Reviews

journal homepage: www.elsevier.com/locate/oregeo

Genesis of the Xinqiao Cu–S–Fe–Au deposit in the Middle-Lower Yangtze River Valley metallogenic belt, Eastern China: Constraints from U–Pb–Hf, Rb–Sr, S, and Pb isotopes

Yu Zhang [a,b,c], Yong-jun Shao [b,c,*], Hong-bin Li [d], Zhong-fa Liu [b,c]

[a] Key Laboratory of Mineralogy and Metallogeny, Guangzhou Institute of Geochemistry, Chinese Academy of Sciences, Guangzhou 510640, China
[b] Key Laboratory of Metallogenic Prediction of Nonferrous Metals and Geological Environment Monitor (Central South University), Ministry of Education, Changsha 410083, China
[c] School of Geosciences and Info-Physics, Central South University, Changsha 410083, China
[d] Graduate School of Engineering and Resource Science, Akita University, Akita 010-0862, Japan

ARTICLE INFO

Article history:
Received 8 November 2015
Received in revised form 9 February 2017
Accepted 13 February 2017
Available online 16 February 2017

Keywords:
Isotope geochemistry
Ore source
Xinqiao Cu–S–Fe–Au deposit
Tongling ore district
Eastern China

ABSTRACT

The Xinqiao Cu–S–Fe–Au deposit in the Tongling ore district, one of important part of Middle-Lower Yangtze River Valley metallogenic belt in Eastern China, is located along the northern margin of the Yangtze craton. It consists of two major types of mineralization: a more economically significant stratiform orebody with pyrite-bearing quartz veins in its footwall, and the less economically important skarn-type orebodies.

An integrated study of zircon U–Pb–Hf and trace elements analysis for the quartz diorite in Xinqiao Jitou stock, Rb–Sr isotope analysis for quartz fluid inclusions from the footwall stockwork mineralization, as well as a systematic S–Pb isotope analysis of sulfides was carried out, all based on detailed field investigations. U–Pb zircon dating of Jitou stock yielded an age of 139.6 ± 1.5 Ma (MSWD = 0.80), close to the Rb–Sr isotope isochron age (138.0 ± 2.3 Ma, MSWD = 5.40, an initial $^{87}Sr/^{86}Sr$ value of 0.71138 ± 0.00014) of quartz fluid inclusions from the footwall stockwork mineralization. The $\varepsilon_{Hf}(t)$ values of zircon grains vary from −15.3 to −8.5 with T_{DM2} ranging from 2151 to 1729 Ma, suggesting that the magma for Jitou stock was probably dominant in crustal-derived magmas with minor mantle material inputs, based on the previous studies on Sr isotope compositions, Nb/Ta ratios and Mg#. The ΔFMQ values (−4.44 to 7.77, average 4.36) suggest that the Jitou stock was derived from the highly oxidized magma and favorable for the Cu mineralization. The systematic S–Pb isotope data and the initial $^{87}Sr/^{86}Sr$ values demonstrate that the stratiform orebody and the footwall stockwork mineralization were likely to be genetically linked to magmatic-hydrothermal events of Yanshanian (Jurassic – Cretaceous) age, as confirmed by closeness of ages of mineralization and magmatism. Therefore, it is interpreted that the Xinqiao stratiform mineralization may have resulted from Yanshanian magmatic hydrothermal fluids associated with the Jitou stock, as may be the case also for the skarn-type mineralization hosted in the contact between the Yanshanian Jitou stock and the Lower Permian Qixia Formation limestone, based on the basis of ore deposit geology. Generally, the Xinqiao Cu–S–Fe–Au mineralization may have been generated by the Yanshanian tectono-thermal event in Eastern China.

1. Introduction

The Tongling ore district in the Middle-Lower Yangtze River Valley metallogenic belt in Eastern China, is located along the northern margin of the Yangtze craton (Fig. 1). It is well-known in China to have widespread Yanshanian granitoids and host numerous skarn type deposits (Mao et al., 2011), such as Tongguanshan, Fenghuanshan and Shizishan Cu deposits. However, the discovery of the large-scale stratiform orebodies in the Xinqiao Cu–S–Fe–Au deposit and the Dongguashan Cu–Au deposit (Fig. 2) has added extra complexities to the regional metallogenesis. The genesis of these stratiform orebodies has been controversial over the past forty years, and is variably argued to be sourced from: 1) Late Paleozoic (Hercynian) submarine exhalation (Fu et al., 1977; Gu et al., 2000; Xu and Zhou, 2001; Xu et al., 2004); 2) Early Cretaceous (Yanshanian) magmatic-hydrothermal fluids (Chang

* Corresponding author at: School of Geosciences and Info-Physics, Central South University, Changsha 410083, China.
E-mail address: shaoyongjun@126.com (Y.-j. Shao).

http://dx.doi.org/10.1016/j.oregeorev.2017.02.014
0169-1368/

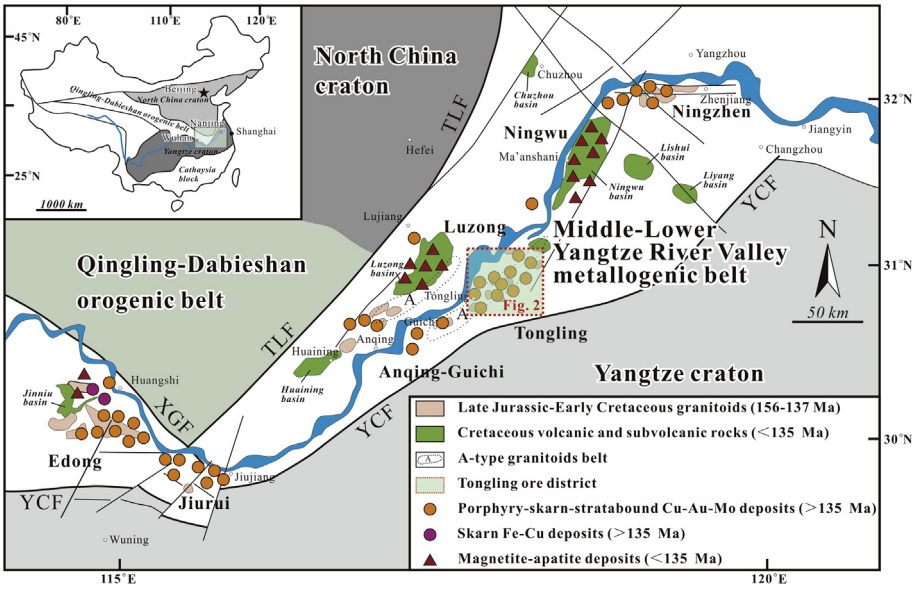

Fig. 1. Location of Tongling ore district in the Middle-Lower Yangtze River Valley metallogenic belt (after Mao et al., 2011). TLF: Tancheng–Lujiang fault; XGF: Xiangfan–Guangji fault; YCF: Yangxing–Changzhou fault.

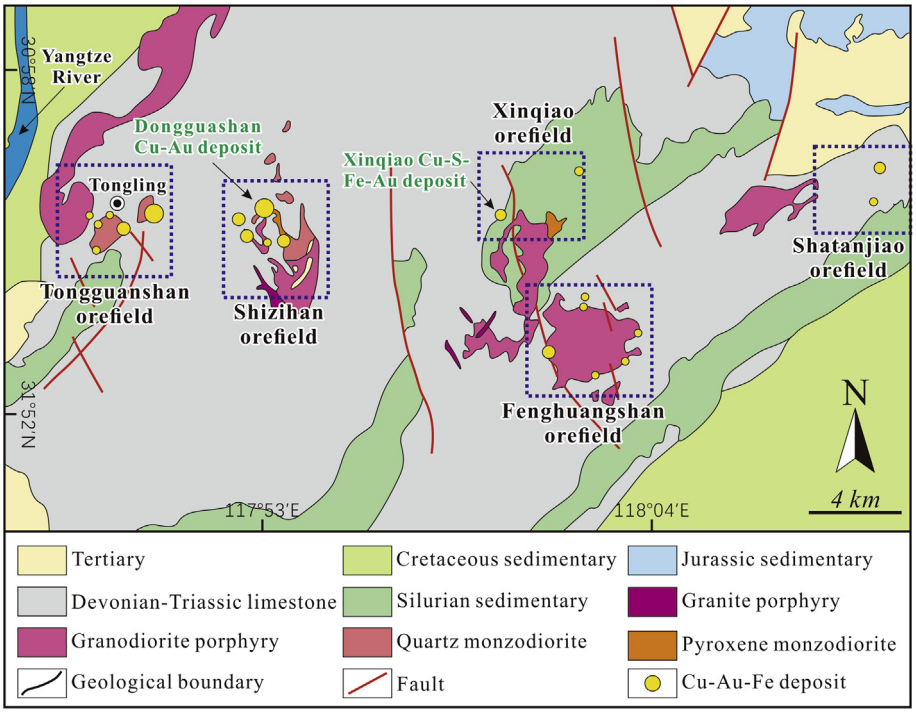

Fig. 2. Geological map of the Tongling district (modified from Chang et al., 1991).

and Liu, 1983; Chang et al., 1991; Zhai et al., 1992; Meng, 1994, 1996; Pan and Done, 1999; Mao et al., 2009, 2011) and 3) Yanshanian magmatism overprinting on Hercynian submarine exhalation mineralization (Yang et al., 1982; Xie et al., 1995; Tang et al., 1998; Zhou et al., 2010; Guo et al., 2011).

The Xinqiao Cu–S–Fe–Au deposit (0.5 Mt Cu @ 0.71%, 75.5 Mt sulfur @ 29.3%, 24.9 Mt Fe @ 46%, 11.2 t Au @ 4.7 g/t and 248.4 t Ag @ 248.4 g/t; Xu and Zhou, 2001) is one of the largest deposit in the Tongling ore district (Fig. 2) and has two major mineralization types: a more economically significant stratiform orebody and the less significant skarn-type orebodies (Fig. 3). In the previous study on the Xinqiao stratiform mineralization, the dacites and the volcaniclastic rocks at the base of the ore-hosting strata (the Upper Carboniferous Huanglong and Chuanshan Formation) and the colloform pyrite were thought to be the direct evidence of the Late Paleozoic submarine exhalative processes (Fu et al., 1977; Gu et al., 2000; Xiao and Ni, 2000; Zhou and Yue, 2000; Xu and Zhou, 2001; Xu et al., 2004). Moreover, the combined Xinqiao stratiform orebody and the footwall stockwork mineralization in the Upper Devonian Wutong Formation quartz sandstone (Fig. 4

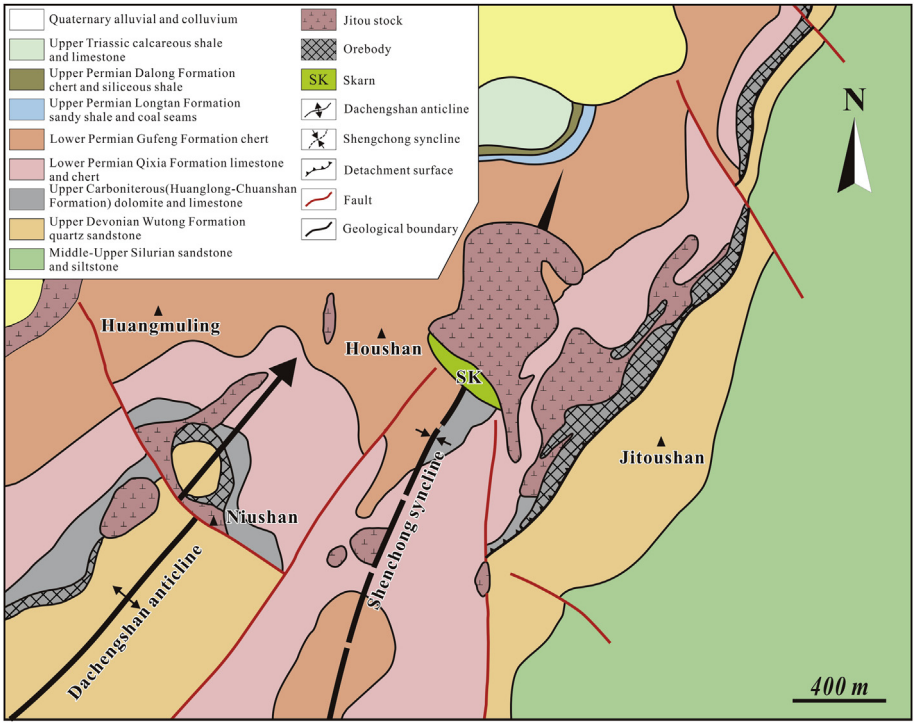

Fig. 3. Geological map of Xinqiao Cu–S–Fe–Au deposit (after Tang et al., 1998).

and Fig. 5a–b) is similar to the dual structure of typical sedimentary exhalative (SEDEX) deposits (Xiao and Ni, 2000; Xu and Zhou, 2001; Xu et al., 2004). Additionally, this hypothesis is further supported by a Re–Os isochron age of 319 ± 13 Ma (late Carboniferous) for pyrites from the footwall stockwork mineralization (Guo et al., 2011).

In contrast, based on studies of the geological characteristics of the Xinqiao deposit and the Tongling ore district, Zhai et al. (1992), Pan and Done (1999) and Mao et al. (2006) suggested that the Xinqiao mineralization may have been generated by the Yanshanian tectono-thermal event in Eastern China and that the stratiform orebody was formed as a result of magmatic-hydrothermal activity along the unconformity between the Upper Devonian Wutong Formation quartz sandstone and the Upper Carboniferous Huanglong Formation dolomite. This unconformity is thought to have acted as a detachment surface during Middle to Late Triassic post-collisional deformation (Fig. 4, Tang et al., 1998; Mao et al., 2009). Mao et al. (2009, 2011) further supported this view because

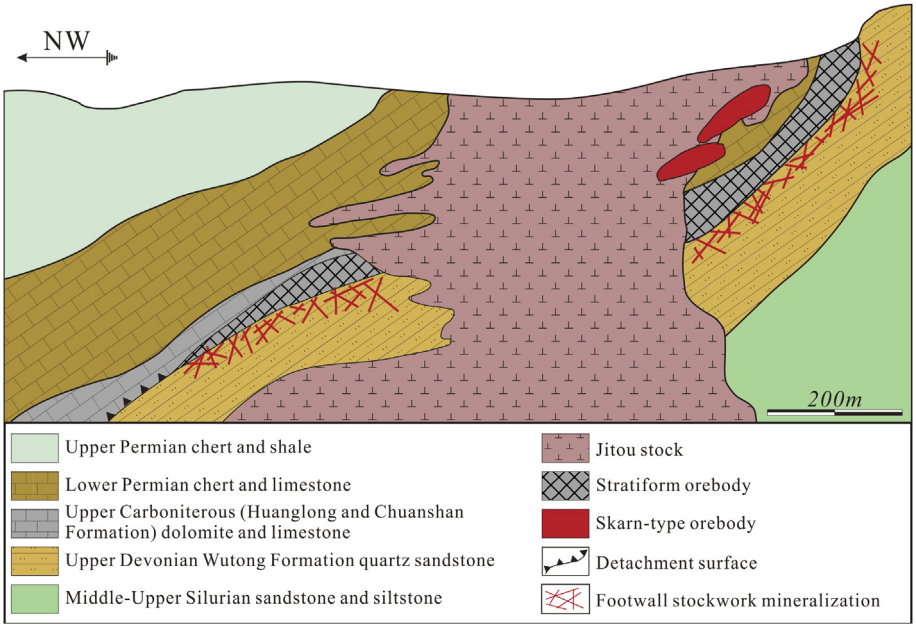

Fig. 4. Representative cross-section through the Xinqiao Cu–S–Fe–Au deposit (after Zang et al., 2004).

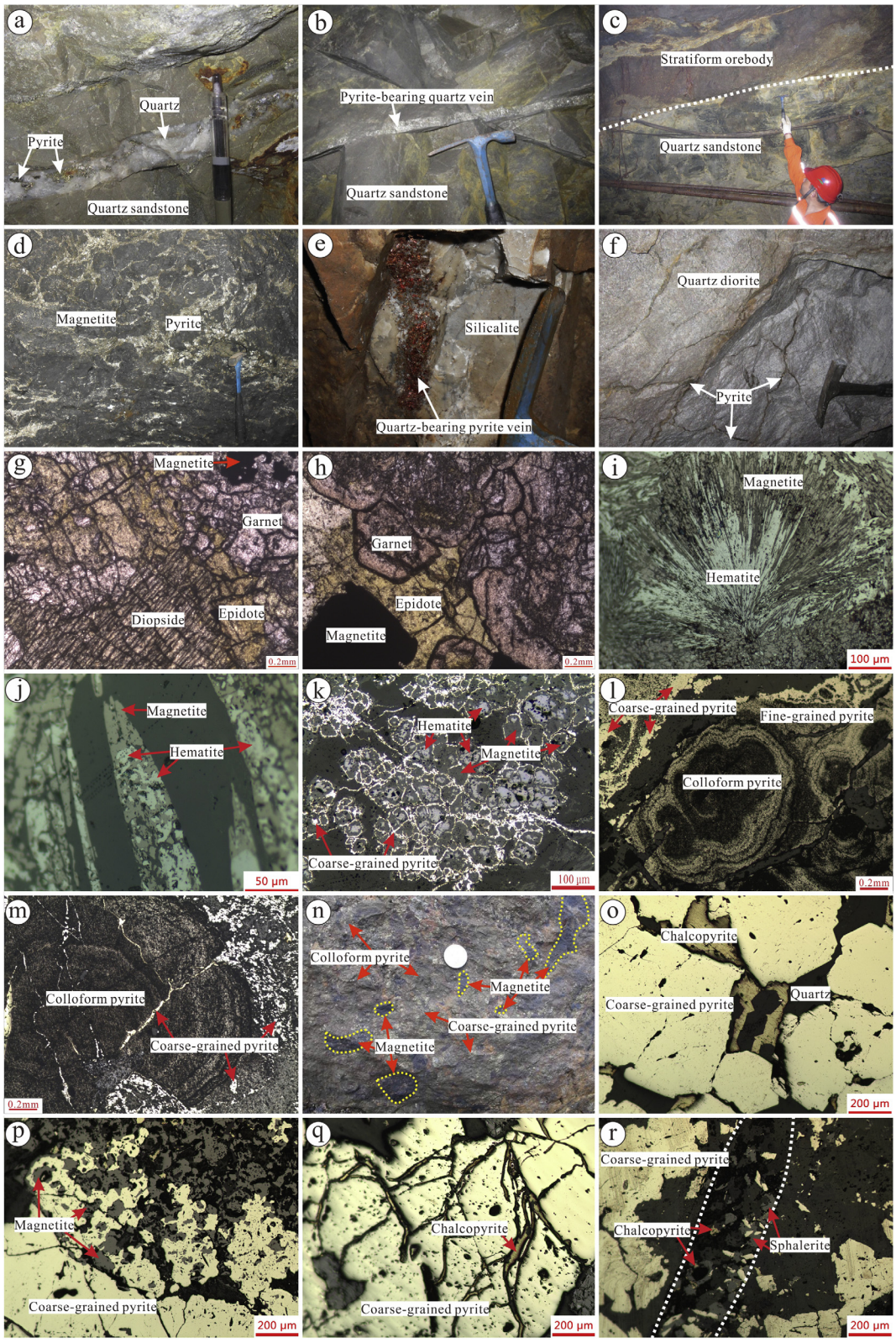

Fig. 5. Photographs showing representative mineral assemblages and textural features of the Xinqiao deposit. (a) and (b) Pyrite-bearing quartz vein in the Wutong Formation quartz sandstone; (c) Sharp contact between the stratiform orebody and the Wutong Formation quartz sandstone; (d) Pyrite crosscutting magnetite in the stratiform orebody; (e) Pyrite vein with a small amount of quartz in the hanging wall of the stratiform orebody (Qixia Formation silicalite), with a surface layer of purple-colored oxide minerals; (f) Veinlet-disseminated pyrite in quartz diorite of the Jitou stock; (g) Garnet and diopside replaced by epidote and locally corroded by magnetite (PPL); (h) Epidote among garnets and locally corroded by magnetite (PPL); (i) Magnetite locally replaced radial hematite; (j) Magnetite locally replaced needle-like hematite; (k) Hematite-bearing magnetite replaced along the edges by pyrite; (l) Colloform pyrite rims recrystallized and changed into fine-grained pyrite, and fine-grained pyrite partially replaced by coarse-grained pyrite; (m) Coarse-grained pyrite vein crosscut colloform pyrite grain; (n) Coarse-grained pyrite and colloform pyrite cement the massive magnetite, indicating that magnetite formed earlier than colloform pyrite; (o) Coarse-grained pyrite coexists with quartz and chalcopyrite in Stage VA; (p) Coarse-grained pyrite replaces magnetite, with some magnetite residues in coarse-grained pyrite; (q) Chalcopyrite stockwork crosscut coarse-grained pyrite; (r) Coarse-grained pyrite + sphalerite + chalcopyrite + quartz veins crosscut quartz-bearing coarse-grained pyrite. (For interpretation of the references to color in this figure legend, the reader is referred to the web version of this article.)

the major alteration mineral assemblage (quartz and pyrite) of the footwall stockwork mineralization is distinct from that of the sedimentary exhalative deposit (anhydrite and barite; Sangester, 1990). The H–O isotope analysis of ore-bearing quartz (Liu, 2002), the Re–Os isochron age (126 ± 11 Ma; Xie et al., 2009) and iron isotope compositions (δ^{57}Fe: −1.22‰ to 0.15‰; Wang et al., 2011, 2013) of pyrites in the stratiform orebody are consistent with the mineralization being resulted from Yanshanian (Jurassic – Cretaceous) magmatic-hydrothermal fluids associated with Jitou stock, but do not exclude the possibility that the orebody was formed via the Yanshanian overprinting on the Hercynian (Late Paleozoic) submarine exhalative processes, the third hypothesis for Xinqiao mineralization (Xie et al., 1995; Tang et al., 1998; Zhou et al., 2010).

To sum up, the genesis of the Xinqiao deposit is poorly constrained, primarily due to uncertainty in whether Late Paleozoic (Hercynian) submarine exhalative mineralization existed. Therefore, in order to understand the genesis of the large-scale stratiform orebodies in the Tongling district clear, we took the Xinqiao Cu–S–Fe–Au deposit as an example and performed in situ U–Pb–Hf and trace elements analysis of zircon from Jitou stock quartz diorite, Rb–Sr isotope analysis of fluid inclusions trapped in quartz from the footwall stockwork mineralization, and systematic S–Pb isotope analysis of sulfides based on detailed field investigations. This study on the Xinqiao Cu–S–Fe–Au deposit aims to constrain the genesis of Xinqiao stratiform mineralization from (1) the relationship between magmatism and mineralization, (2) the source of ore-forming materials, (3) the age of Xinqiao mineralization and (4) the genesis of footwall stockwork mineralization.

2. Geological setting

2.1. Regional geology

The Yangtze block is separated from the North China Craton by the Triassic Dabie orogenic belt to the north, and from the Cathaysian block by the Neoproterozoic suture to the south (Fig. 1; Li et al., 2014). The Middle-Lower Yangtze River Valley metallogenic belt is located in the Yangtze block and famous for its abundant (more than 200) polymetallic deposits (Ling et al., 2009). The Tongling ore district, located in the central part of the Middle-Lower Yangtze River Valley metallogenic belt (Fig. 1), is the largest Cu–Au–Fe–Mo ore district in the belt and well-known in China to host numerous skarn deposits (Tang et al., 1998; Pan and Done, 1999; Lai and Chi, 2007; Mao et al., 2011). More than 50 ore deposits have been discovered in the Tongling district (Wu et al., 2014), and they are clustered in five orefields distributed from east to west, namely Tongguanshan, Shizishan, Xinqiao, Fenghuangshan and Shatanjiao, respectively (Fig. 2). The dominant lithologies in the Tongling district are marine and continental sedimentary rocks. Marine sedimentary rocks including clastic sedimentary rocks, carbonates, and evaporites, were deposited in the Silurian–Middle Triassic, with the exception of the Early–Middle Devonian. Continental rocks include clastic and volcanic sedimentary rocks ranging from Middle Jurassic to Quaternary, excluding the Middle-Late Devonian (Wang et al., 2015; Cao et al., 2017). The sedimentary rocks are developed on a stable Precambrian basement, forming a thick sequence that became the country rocks for later Cu, Au, Fe, and Mo mineralization (Chang et al., 1991; Zhai et al., 1992; Cao et al., 2017). The Lower Permian Qixia Formation and the Lower Triassic Nanlinghu Formation are dominated by limestone and important ore-hosting rocks of the widespread skarn mineralization in this district, and the unconformity between the Upper Devonian Wutong Formation quartz sandstone and the Upper Carboniferous Huanglong Formation dolomite and limestone, constrains the economically significant stratiform mineralization in this district, such as the Xinqiao and Dongguashan deposits. Structurally, the region contains NE-trending folds and NNE- and NW-trending faults which control the intrusion emplacement. Igneous rocks are widely distributed in the region, including more than 70 intrusions and making up approximately 10% of the area, and are dominated by Late Jurassic – Early Cretaceous (ca. 156–137 Ma) high-K calc-alkaline intermediate granitoids (e.g., granite porphyry, granodiorite porphyry and quartz monzodiorite) (Fig. 2; Mao et al., 2011; Wang et al., 2015; Cao et al., 2017). Many small plutons with surface exposures from 0.15 to 5.00 km^2 occur as composite stocks, dikes and sills in this region (Du et al., 2015).

2.2. Ore deposit geology

The Xinqiao Cu–S–Fe–Au deposit is situated 24 km east of Tongling city, Anhui Province, China. The sedimentary rocks that crop out in the mining area are from the Middle – Upper Silurian sandstone and siltstone to Lower Triassic Yinkeng Formation limestone, whereas the Lower Carboniferous unit is absent in the deposit area. Major structures at Xinqiao are the NE-oriented Dachengshan anticline and the NNE-oriented Shenchong syncline (Fig. 3), and the joint of the two folds is the advantageous location of magmatic rocks and orebody (Fig. 3). The dominant igneous rock in the region is the Jitou stock, which is associated with the skarn in the area and composed of quartz diorite at the center and diorite porphyry along the edges. The Jitou stock has a SHRIMP zircon U–Pb age of 140.4 ± 2.2 Ma (Wang et al., 2004).

The stratiform orebody with 90% of reserves is constrained in the detachment zone between the Upper Devonian Wutong Formation and the Upper Carboniferous Huanglong Formation (Fig. 4). The Upper Carboniferous Huanglong and Chuanshan Formation are mainly composed of dolomite and limestone, respectively, in which the Huanglong dolomite was extensively replaced by the stratiform orebody. The Upper Devonian Wutong Formation, dominated by quartz sandstone, acts as the footwall of the stratiform orebody, in which there are pyrite-bearing quartz stockwork veins at the contact with the stratiform orebody (Fig. 5a, b). The Lower Permian Qixia Formation, composed of limestone and chert, is the hanging wall of the stratiform orebody. The stratiform orebody is 2560 m long and 1810 m wide, averaging 21 m in thickness, striking NE and dipping to northwest, parallels to the strata of the Upper Devonian Wutong Formation and the Upper Carboniferous Huanglong Formation (Fig. 4) and has obvious abrupt contact with quartz sandstone of Wutong Formation (Fig. 5c).

Field and microscopy observations indicate that ore minerals in the stratiform orebody are magnetite, chalcopyrite, pyrrhotite, hematite, native gold and electrum, with gangue minerals including garnet, diopside, epidote, chlorite, quartz and calcite. We found that the metallic mineral assemblages in the stratiform orebody show proximal to distal zoning: Jitou stock → magnetite + pyrite → chalcopyrite + pyrite → pyrite. Pyrite occurs mainly in five settings as the most widely distributed ore mineral in the Xinqiao region, namely, (1) in the stratiform orebody (Fig. 5d); (2) in quartz veins of the footwall stockwork mineralization (Fig. 5a, b); (3) in quartz veins in the hanging wall of the stratiform orebody (Fig. 5e); (4) in the skarn-type orebodies; and (5) veinlet-disseminated pyrite in the Jitou stock (Fig. 5f).

Based on the mineral assemblages and textural relationships, the stratiform mineralization at Xinqiao comprises five stages (Fig. 6), namely the early skarn (Stage I), late skarn (Stage II), iron oxides (Stage III), colloform pyrite (Stage IV) and the quartz-sulfide (Stage V). Stage III can be further divided into a hematite (Stage IIIA) and magnetite (Stage IIIB) sub-stages, and Stage V can be further divided into a quartz-pyrite (Stage VA) and

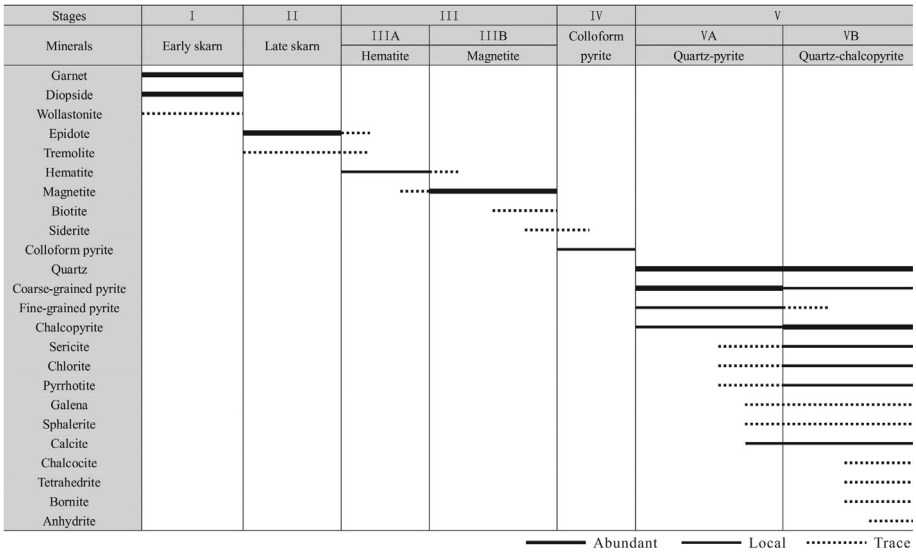

Fig. 6. Mineral paragenesis of the Xinqiao stratiform mineralization.

quartz-chalcopyrite (Stage VB) sub-stages (Zhang, 2015). *Stage I* is dominated by abundant garnet and diopside coexisting with trace wollastonite (Xie, 2012). Garnet is euhedral or anhedral granular texture (Fig. 5g, h). Diopside is mainly subhedral granular or allotriomorphic prismatic texture (Fig. 5g). Locally, garnet and diopside were replaced by epidote and corroded by magnetite (Fig. 5g, h), which indicates that epidote and magnetite were formed later than garnet and diopside. *Stage II* is characterized by abundant epidote, most of which contains allotriomorphic texture and occurs within the Stage I garnet grains (Fig. 5h). Some epidotes locally replaced garnet and diopside pseudomorphs (Fig. 5g). *Stage IIIA* is mainly composed of radial or needle-like hematite, whose pseudomorphs were usually replaced in by later magnetite (Fig. 5i, j). *Stage IIIB* (magnetite) is the most important Fe mineralization stage, in which massive magnetite was cut by Stage V pyrite veins (Fig. 5d). Hematite-bearing magnetite grains were locally replaced by late pyrite along the grain boundaries (Fig. 5k). *Stage IV* is characterized by colloform pyrite. A single pyrite grain shows typical colloform or concentric ring textures (Fig. 5l, m). The majority of colloform pyrite has experienced recrystallization and transformed into Stage VA fine-grained pyrite, which commonly has metasomatic relict texture (Fig. 5l). The colloform pyrite grains are locally cut by the Stage V coarse-grained pyrite veins (Fig. 5m). In addition, colloform pyrites and coarse-grained pyrites were also found to cement Stage IIIB massive magnetite (Fig. 5n), which provides good evidence for the colloform Py1 forming after magnetite. *Stage VA* is characterized by abundant coarse-grained pyrites coexisting with abundant quartz and minor fine-grained pyrites (Fig. 5l) and chalcopyrite (Fig. 5o). Coarse-grained pyrites locally replace magnetite (Fig. 5p). *Stage VB* is the main Cu mineralization stage and contains abundant quartz, calcite, chalcopyrite and pyrite, together with minor pyrrhotite, galena, sphalerite, sericite and chlorite. Guo et al. (2011) and Xie (2012) reported that trace Cu-bearing sulfides (e.g., chalcocite, tetrahedrite and bornite) and anhydrite were formed at this sub-stage. Chalcopyrite mainly occurs as allotriomorphic texture. Chalcopyrite stockwork locally crosscut Stage VA coarse-grained pyrites (Fig. 5q). Sphalerite locally occurs as veins together with pyrite, chalcopyrite and quartz (Fig. 5r).

The detailed field investigation indicates that the wall rock of the stratiform orebody typically include garnet, sericitic, silicic, chloritic and argillic alteration, and chert is only developed in the footwall of the stratiform orebody (Fig. 5a, b).

The skarn-type orebodies (not yet mined), which account for 10% of the mineralization in the Xinqiao deposit, are developed at the contact zone between the Jitou stock and the Lower Permian Qixia Formation limestone. The endoskarn and exoskarn are both calcitic skarn consisting predominately of garnet, wollastonite and subordinate pyroxene (Wang et al., 2011). The main metallic minerals of the skarn-type orebodies are magnetite, pyrite, chalcopyrite, pyrrhotite, sphalerite and galena with massive, veins and disseminations.

3. Sampling and analytical methods

3.1. U–Pb dating and trace elements analysis of zircon

A quartz diorite sample (XQ33-10) was collected from Jitou stock at an underground depth of −270 m for zircon U–Pb dating. The sample (Fig. 7a) displays the weak chloritic and silicic alteration and consists of plagioclase, hornblende, and quartz with minor K-feldspar and accessory titanite, apatite, and zircon. Plagioclase grains are subhedral to anhedral, 0.4–1.3 mm in size and show polysynthetic twins and zonal textures (Fig. 7b). Hornblende grains are anhedral to subhedral and 0.1–0.4 mm in size (Fig. 7c).

Zircon grains were extracted from ~5 kg of whole-rock samples by standard crushing, sieving, and heavy liquid and magnetic separation techniques, and were then mounted on double-sided tape, cast in epoxy resin, and polished to expose surfaces suitable for analysis by laser ablation-inductively coupled plasma-mass spectrometry (LA-ICP-MS). The zircon mounts were cleaned in a 3% HNO_3 bath with an ultrasonic wash prior to LA-ICP-MS analysis. Cathodoluminescence (CL) images were taken of all zircon grains at Linghang Co. Ltd., Beijing, China, using a JEOL JXA-8100 electron microprobe.

Zircon U–Pb isotope and trace elements analysis were carried out using an LA-ICP-MS at the Testing Center, Shandong Bureau of China Metallurgical Geology Bureau (Jinan, China). Ablation was achieved using a pulsed 193 nm ArF Excimer (COMPexPRO CO_2F Geolas) with a laser power of 8.5 J/cm^2 pulse energy at a repetition rate of 8 Hz, coupled to an Agilent 7500a quadrupole ICP-MS. Helium was used as a carrier gas to provide efficient aerosol transport to the ICP and to minimize aerosol deposition. The diameter of the laser ablation crater was 30 μm. The total ablation time was 110 s, including 30 s for the blank signal, 55 s for ablation, and

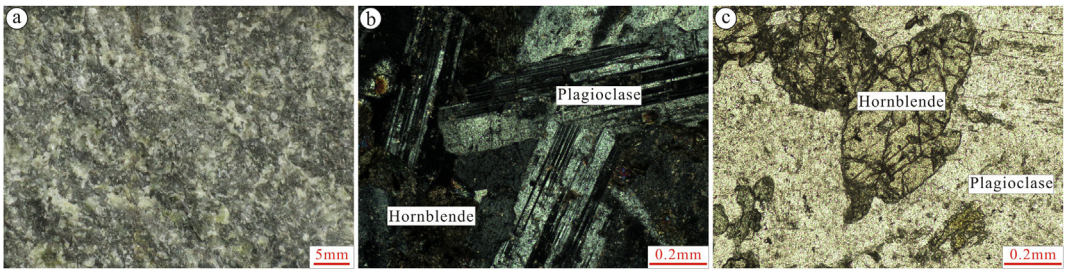

Fig. 7. (a) Hand-specimen photograph of quartz diorite with weak chloritic and silicic alteration; (b) and (c) Transmitted light photomicrographs of quartz diorite in the Jitou stock, showing plagioclase with polysynthetic twinning (cross-polarized light) and anhedral hornblende (plane-polarized light), respectively.

25 s for the residual signal. To correct laser-induced fractionation, Zircon 91500 was used as an external standard to normalize isotopic fractionation during isotope analysis. The standard was analyzed twice in every five analyses. An external standard of Nist610 glass was analyzed once in every 10 analyses to normalize U, Th, Pb and other trace elements. The resultant data were processed using ICPMSDataCal (Liu et al., 2010).

3.2. Hf isotope analysis of zircon

The sites of Hf isotope analysis are the same as those of the U–Pb isotope and trace elements analysis. These analyses were performed using Neptune Plus multicollector ICP-MS (MC-ICP-MS) (Thermo Fisher Scientific, Germany) in combination with a Geolas 2005 excimer ArF laser ablation system (Lambda Physik, Göttingen, Germany) at the State Key Laboratory of Geological Processes and Mineral Resources, China University of Geosciences, Wuhan, China. This laser ablation system includes a "wire" signal smoothing device, which enables steady signals to be produced even at laser repetition rates as low as 1 Hz. The energy density of laser ablation used in this study was 5.3 J/cm^2. Helium was used as the carrier gas within the ablation cell and was merged with argon (makeup gas) after the ablation cell. Helium achieved a consistent twofold signal enhancement for the 193 nm laser over argon gas. We used a simple Y junction downstream from the sample cell to add small amounts of nitrogen (4 ml min^{-1}) to the argon makeup gas flow. Compared with the standard arrangement, the addition of nitrogen together with the newly designed X skimmer cone and Jet sample cone in the Neptune Plus improved the signal intensity of Hf, Yb, and Lu by factors of 5.3, 4.0 and 2.4, respectively. All data in this study were acquired on zircon grains in single spot ablation mode using a spot size of 44 μm. Each measurement consisted of 20 s of acquisition of the background signal followed by 50 s of acquisition of the ablation signal. Detailed operating conditions for the laser ablation system and the MC-ICP-MS instrument and analytical method are given in Hu et al. (2012). Off-line selection and integration of analytic signals and mass bias calibrations were performed using ICPMSDataCal (Liu et al., 2010).

3.3. Rb–Sr isotope analysis of quartz fluid inclusions

Samples for Rb–Sr isotope analysis were collected from pyrite-bearing quartz veins in quartz sandstone of Wutong Formation (Fig. 5a, b) that form the footwall stockwork mineralization of the stratiform orebody. To avoid altered samples by magmatic-hydrothermal fluids and to simplify the discussion on the genesis of the footwall stockwork mineralization, the samples were collected far from the stratiform orebody and the Jitou stock, and narrower veins were preferentially sampled. Sample locations are listed in Table 1.

Quartz grains were extracted from the quartz-bearing pyrite ores by conventional techniques including crushing, oscillation, heavy liquid and magnetic separation, and were then handpicked under a microscope to at least 99% purity. The Rb–Sr isotope analysis of quartz fluid inclusions were carried out in the ALS European Isotopic Laboratory, Lulea, Sweden. The quartz grains were first washed twice with 6 mol/L HCl and then washed with distilled water to neutral pH. After drying, the secondary inclusions in quartz were cleaned by the thermal explosion and ultrasonic washing method. Lithium tetraborate was used to fuse the quartz, Rb and Sr were separated and purified by the ion exchange method. Rb and Sr contents were measured by high resolution sector magnetic field plasma mass spectrometry (ID-ICP-SFMS), and $^{87}Rb/^{86}Sr$ and $^{87}Sr/^{86}Sr$ were measured by MC-ICP-MS. The contents and isotopic ratio were measured following the detailed analytical procedures outlined in Wang et al. (2007). The $^{87}Sr/^{86}Sr$ ratio of the American isotopic standard (NBS987) is determined as 0.710233 ± 3 (1σ), and the uncertainties (1σ) of $^{87}Rr/^{86}Sr$ are 0.5%. The Rb–Sr isochron ages were calculated using isoplot software (Version 3.75) (Ludwig, 2012) with a 2σ index for the dating error and values of $\lambda_{Rb} = 1.42 \times 10^{-11}$ a^{-1} (Wang et al., 2007).

3.4. S–Pb isotope analysis of sulfides

Samples for S–Pb isotope analysis were collected from the stratiform orebody, the footwall stockwork mineralization, the skarn-type orebodies, disseminated pyrite in quartz diorite from the Jitou stock and from the pyrite-bearing quartz veins in the Lower Permian Qixia Formation that forms the hanging wall of the stratiform orebody. Most of the S–Pb isotope analyses were carried out on pyrite, although some were also carried out on galena, sphalerite and pyrrhotite from the stratiform orebody. Two samples of magnetite in the stratiform orebody were collected for Pb isotope analysis.

Table 1
Locations of samples collected for Rb–Sr isotope analysis.

No.	Sample	Sample characteristic	Sample location
1	XQ030-6-1	Quartz-bearing pyrite ore	No. 4 transverse drift, −300 m mining level
2	XQ030-6-2	Quartz-bearing pyrite ore	No. 4 transverse drift, −300 m mining level
3	XQ031-2	Quartz-bearing pyrite ore	No. 5 transverse drift, −300 m mining level
4	D005-1	Quartz-bearing pyrite ore	W401 stope, −300 m mining level
5	D011-1	Quartz-bearing pyrite ore	W513 stope, −270 m mining level
6	D011-2	Quartz-bearing pyrite ore	W513 stope, −270 m mining level

Sulfide minerals were handpicked under a microscope to at least 99% purity after crushing, centrifugation, heavy liquid and magnetic separation. S and Pb analyses were carried out at Analysis and Testing Center, Beijing Institute of Geology for Nuclear Industry, Beijing, China. The S isotope ratios were measured using a Finningan Mat-251 EM mass spectrometer and the results are reported in standard δ notation in per mil (‰) relative to the Canyon Diablo Troilite (CDT) standard. The reproducibility of the $\delta^{34}S$ value is ±0.2‰. For Pb analysis, sample powders were dissolved in HF–HNO_3–$HClO_4$ mixture. The digested samples were then dried, dissolved in 6 mol/L HCl and dried again, and then dissolved in 0.5 mol/L HBr solution for Pb separation. The Pb fraction was separated using strong alkali-anion exchange resin with HBr and HCl as eluents. The analysis was carried out by thermal ionization mass-spectrometry using a Triton mass spectrometer. The detailed analytical procedures were outlined in Wang et al. (2016).

4. Results

4.1. U–Pb dating and trace elements analysis of zircon

CL images show that zircon grains from quartz diorite sample XQ33-10 display a narrow oscillatory zoning, are subhedral to anhedral, have tetragonal dipyramid shapes, and are 50–60 μm in size (Fig. 8a). Twenty zircon grains were selected for U–Pb isotope and trace elements analysis; the results are given in Tables 2 and 3. All the zircon grains analyzed are LREE-depleted, HREE-rich with positive Ce anomalies (Ce/Ce^* = 5.50–71.35, average 32.63) as well as negative Eu anomalies (Eu/Eu^* = 0.44–0.69, average 0.57), which indicate that the zircon grains analyzed are magmatic in origin (Fig. 8b; Table 3; Zhao, 2010). This interpretation is also supported by Th/U ratios ranging from 0.69 to 1.76 (average 1.07). Twenty zircon grains yielded $^{206}Pb/^{238}U$ ages of ca. 146.1–131.8 Ma and a weighted mean age of 139.6 ± 1.5 Ma (MSWD = 0.80) (Fig. 8c, d; Table 2). This latter age represents the age of crystallization of the Jitou stock and is similar to the Ar–Ar age of 137 ± 1 Ma (Zhou and Yue, 2000) and the SHRIMP U–Pb age of 140.4 ± 2.2 Ma (Wang et al., 2004). Therefore, from the aforementioned, the Jitou stock formed in the early Cretaceous.

The Ti-in-zircon thermometer can be used to determine temperatures of the magma (Watson et al., 2006), with the detailed calculation being presented by Watson et al. (2006). In this study, the calculated Ti-in-zircon temperatures of Jitou stock quartz diorite are ca. 695–837 °C (avg. 780 °C) (Table 3). The oxygen fugacity of magmatic melt based on the incorporation of cerium into zircon and Ti-in-zircon temperature, and the detail calibration has been presented by Trail et al. (2011). In this study, the calculated log (fO_2) and ΔFMQ of the magma for the Jitou stock ranges from −19.84 to −7.35 (average −10.85; Table 3), −4.44 to 7.77 (average 4.36; Table 3), respectively.

4.2. Hf isotope compositions

A total of 14 LA-MC-ICP-MS spot analyses were made. All $^{176}Lu/^{177}Hf$ ratios are <0.002 (0.001109–0.001866; Table 4), indicating that time-integrated changes to the $^{176}Hf/^{177}Hf$ as a result of *in-situ* ^{176}Lu decay is negligible (Wu et al., 2007), which suggests that the zircon grains analyzed have preserved the initial

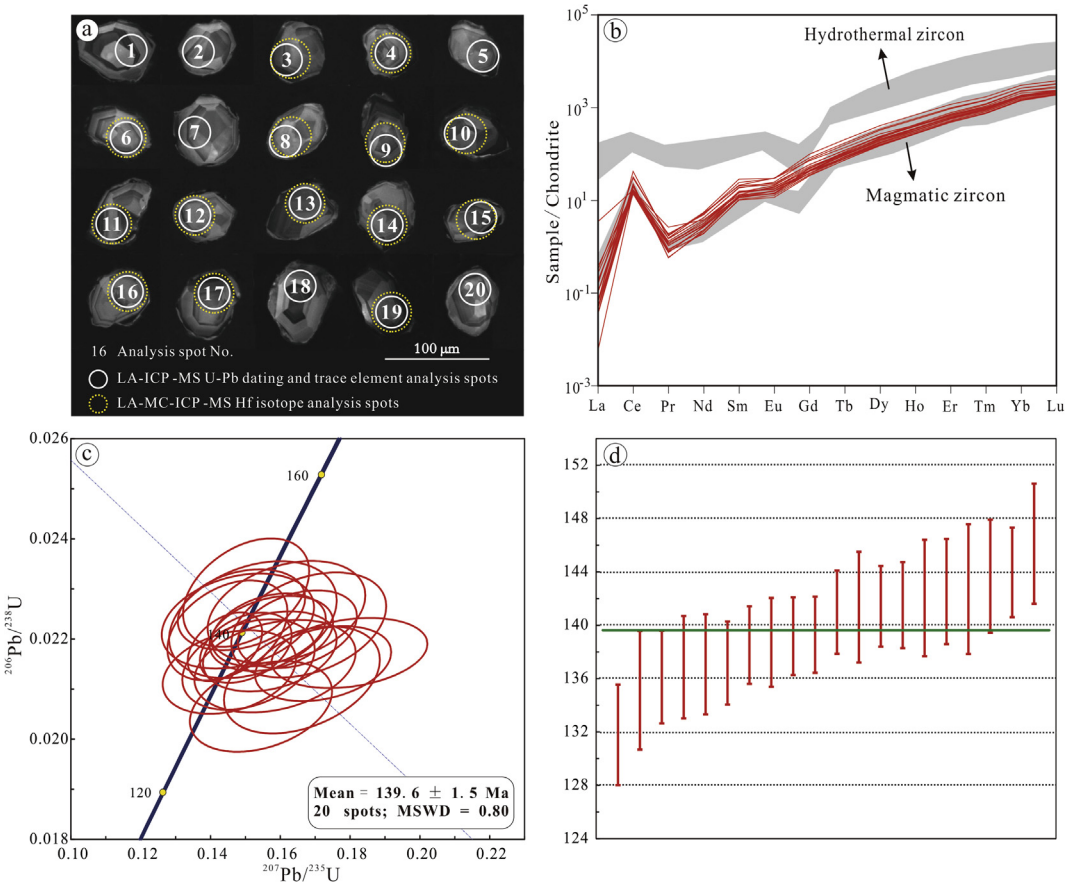

Fig. 8. (a) CL images of zircon grains analyzed by LA-ICP-MS; (b) Chondrite-normalized REE patterns of zircon grains from quartz diorite in the Jitou stock, analyzed by LA-ICP-MS. Chondrite values are from Sun and McDonough (1989); (c) zircon U–Pb concordia diagram for the Xinqiao quartz diorite; (d) zircon weighted mean $^{206}Pb/^{238}U$ ages for the Xinqiao quartz diorite.

Table 2
LA-ICP-MS zircon U–Pb data of quartz diorite from the Jitou stock.

No.	Pb (ppm)	Th (ppm)	U (ppm)	Th/U	Isotope ratios			Age(Ma)		
					$^{207}Pb/^{206}Pb \pm \sigma$	$^{207}Pb/^{235}U \pm \sigma$	$^{206}Pb/^{238}U \pm \sigma$	$^{206}Pb/^{238}U \pm \sigma$	$^{207}Pb/^{235}U \pm \sigma$	$^{207}Pb/^{206}Pb \pm \sigma$
1	7	256	219	1.17	0.0528 ± 0.0041	0.1570 ± 0.0126	0.0218 ± 0.0005	138.7 ± 3.3	148.1 ± 11.1	320.4 ± 184.2
2	4	133	134	0.99	0.0550 ± 0.0046	0.1545 ± 0.0134	0.0207 ± 0.0006	131.8 ± 3.8	145.9 ± 11.8	413.0 ± 188.9
3	4	118	125	0.95	0.0487 ± 0.0045	0.1479 ± 0.0144	0.0224 ± 0.0006	142.5 ± 3.9	140.0 ± 12.7	200.1 ± 142.6
4	3	111	113	0.98	0.0598 ± 0.0057	0.1662 ± 0.0147	0.0212 ± 0.0007	135.1 ± 4.4	156.1 ± 12.8	598.2 ± 207.4
5	5	187	166	1.13	0.0499 ± 0.0044	0.1489 ± 0.0120	0.0226 ± 0.0005	144.0 ± 3.4	140.9 ± 10.6	190.8 ± 192.6
6	4	158	147	1.08	0.0522 ± 0.0047	0.1509 ± 0.0125	0.0215 ± 0.0006	137.1 ± 3.8	142.7 ± 11.0	300.1 ± 207.4
7	4	113	159	0.71	0.0515 ± 0.0048	0.1454 ± 0.0126	0.0213 ± 0.0006	136.1 ± 3.5	137.9 ± 11.2	264.9 ± 216.6
8	5	141	148	0.96	0.0483 ± 0.0038	0.1502 ± 0.0119	0.0229 ± 0.0007	146.1 ± 4.5	142.1 ± 10.5	122.3 ± 177.8
9	4	137	143	0.96	0.0581 ± 0.0042	0.1723 ± 0.0129	0.0215 ± 0.0005	137.2 ± 3.1	161.4 ± 11.1	600.0 ± 161.1
10	7	305	235	1.30	0.0523 ± 0.0037	0.1567 ± 0.0108	0.0222 ± 0.0005	141.4 ± 3.0	147.8 ± 9.5	298.2 ± 164.8
11	8	380	247	1.54	0.0521 ± 0.0042	0.1575 ± 0.0117	0.0221 ± 0.0005	141.0 ± 3.1	148.5 ± 10.3	300.1 ± 185.2
12	4	121	127	0.95	0.0488 ± 0.0042	0.1449 ± 0.0114	0.0222 ± 0.0007	141.4 ± 4.2	137.4 ± 10.1	200.1 ± 127.8
13	10	424	304	1.40	0.0502 ± 0.0029	0.1501 ± 0.0087	0.0218 ± 0.0005	139.2 ± 2.9	142.0 ± 7.7	211.2 ± 135.2
14	4	133	119	1.12	0.0546 ± 0.0053	0.1585 ± 0.0152	0.0215 ± 0.0006	136.9 ± 3.8	149.4 ± 13.4	398.2 ± 223.1
15	6	170	195	0.87	0.0599 ± 0.0049	0.1799 ± 0.0147	0.0217 ± 0.0005	138.5 ± 2.9	167.9 ± 12.7	598.2 ± 177.8
16	3	103	113	0.92	0.0600 ± 0.0064	0.1682 ± 0.0147	0.0223 ± 0.0007	142.0 ± 4.4	157.8 ± 12.7	611.1 ± 231.5
17	4	127	121	1.05	0.0518 ± 0.0047	0.1618 ± 0.0149	0.0225 ± 0.0007	143.7 ± 4.2	152.3 ± 13.0	279.7 ± 207.4
18	15	749	426	1.76	0.0480 ± 0.0024	0.1441 ± 0.0070	0.0218 ± 0.0005	139.3 ± 2.9	136.7 ± 6.3	101.9 ± 114.8
19	6	149	216	0.69	0.0540 ± 0.0036	0.1649 ± 0.0113	0.0222 ± 0.0005	141.5 ± 3.2	155.0 ± 9.8	372.3 ± 151.8
20	4	115	125	0.92	0.0542 ± 0.0066	0.1522 ± 0.0159	0.0224 ± 0.0008	142.7 ± 4.9	143.8 ± 14.0	388.9 ± 275.9

Table 3
LA-ICP-MS trace elements data of zircon from quartz diorite in the Jitou stock (ppm).

No.	Ti	La	Ce	Pr	Nd	Sm	Eu	Gd	Tb	Dy	Ho	Er	Tm	Yb	Lu	T (°C)	log (fO_2)	FMQ buffer	ΔFMQ
1	15.183	0.012	19.172	0.105	1.377	2.354	1.155	11.889	4.432	56.210	23.160	118.457	29.011	317.334	63.862	779	−8.05	−15.21	7.16
2	22.410	0.020	13.370	0.126	1.701	2.959	1.273	13.315	4.297	54.016	21.936	109.689	27.405	298.077	58.468	817	−9.03	−14.38	5.35
3	13.608	0.016	13.157	0.089	1.650	2.432	1.004	11.984	4.030	50.436	20.651	104.881	25.535	271.053	58.643	769	−10.25	−15.44	5.19
4	16.286	0.033	18.156	0.139	1.925	3.142	1.305	14.935	5.355	65.746	26.510	132.642	31.899	349.585	68.314	786	−10.44	−15.06	4.62
5	27.150	0.084	15.998	0.127	1.775	2.497	1.188	13.546	4.697	59.499	25.275	128.039	31.446	339.552	72.665	837	−10.24	−13.97	3.73
6	20.699	0.033	13.016	0.095	1.146	2.089	0.937	11.057	3.693	47.891	20.592	104.403	25.792	281.392	60.143	809	−9.88	−14.55	4.67
7	7.535	0.002	14.707	0.137	2.119	2.659	1.461	13.779	4.841	59.861	23.842	121.120	30.337	334.379	64.898	717	−9.16	−16.70	7.54
8	22.957	0.117	14.816	0.185	3.204	4.126	1.705	18.396	6.084	71.831	28.776	139.302	33.175	354.252	71.479	820	−12.60	−14.33	1.73
9	13.825	0.055	15.542	0.149	1.890	2.917	1.391	15.771	4.953	62.718	25.182	127.261	30.813	336.721	69.392	770	−12.84	−15.41	2.56
10	17.162	0.022	21.592	0.069	1.363	2.502	1.007	15.510	5.575	74.448	31.668	164.984	40.264	440.799	88.360	791	−7.46	−14.95	7.49
11	22.869	0.099	28.432	0.217	3.035	4.255	2.211	25.627	8.693	107.037	42.899	208.674	48.589	503.448	102.763	819	−10.15	−14.34	4.19
12	13.839	1.110	15.796	0.317	2.277	2.624	1.156	11.733	3.973	48.971	20.374	103.704	24.916	283.364	58.270	770	−19.84	−15.40	−4.44
13	14.204	0.049	30.436	0.206	3.320	5.753	2.17	30.791	10.314	127.184	51.337	247.373	56.736	581.648	118.043	773	−10.58	−15.35	4.77
14	5.767	0.034	15.378	0.182	2.529	3.836	1.606	18.401	5.998	75.365	29.824	145.404	34.090	355.082	73.614	695	−16.27	−17.27	1.00
15	10.703	0.059	16.084	0.230	2.933	4.862	2.17	22.321	6.899	84.592	30.878	148.251	35.747	394.406	74.126	747	−14.80	−15.95	1.15
16	15.410	0.056	14.862	0.094	1.174	2.019	0.849	10.528	3.733	46.791	19.772	101.296	24.749	270.130	58.279	781	−11.71	−15.18	3.47
17	14.390	0.011	14.168	0.159	2.264	2.992	1.539	16.745	5.226	65.614	25.756	125.841	30.256	328.343	68.100	774	−10.13	−15.32	5.20
18	15.039	0.021	39.828	0.178	2.549	3.714	1.813	23.575	7.904	101.602	40.547	199.617	47.456	504.215	99.724	778	−7.46	−15.23	7.77
19	11.922	0.016	20.407	0.071	1.277	2.370	1.045	13.950	5.133	69.136	29.683	154.687	38.579	431.069	83.282	757	−8.76	−15.72	6.97
20	22.579	0.014	15.602	0.098	1.592	2.248	1.056	13.008	4.08	53.214	21.786	110.818	27.598	299.843	61.130	818	−7.35	−14.36	7.01

Note: T (°C) is the Ti temperature of zircon, as calculated using the formula of Watson et al. (2006); log(fO_2) and FMQ buffer were calculated following Trail et al. (2011). ΔFMQ = log(fO_2) − FMQ buffer.

$^{176}Hf/^{177}Hf$ from the source and can be used to determine the Hf isotope composition of the source at the time of crystallization. The zircon grains have initial $^{176}Hf/^{177}Hf$ values of 0.282255–0.282447, $\varepsilon_{Hf}(t)$ values of −15.3 to −8.5, and two-stage Hf model ages (T_{DM2}) of 2151–1729 Ma.

4.3. Rb–Sr dating

Rb and Sr in quartz occur only in fluid inclusions (Rossman et al., 1987), so Rb–Sr isotope compositions obtained by analyzing fused glass beads reflect those of the ore-forming fluids and Rb–Sr dating of quartz yields the age of ore-forming events. In the analyzed samples, Rb and Sr concentrations are 1.250–9.020 and 2.723–5.710 ppm, respectively (Table 5). $^{87}Rb/^{86}Sr$ ratios range from 1.009 to 5.577 (average 4.045) and $^{87}Sr/^{86}Sr$ ratios range from 0.713404 to 0.722375 (average 0.719314). A diagram of $^{87}Rb/^{86}Sr$ versus $^{87}Sr/^{86}Sr$ (Fig. 9) yields a Rb–Sr isotope isochron age for quartz fluid inclusions of 138.0 ± 2.3 Ma (MSWD = 5.40), and the initial value of $^{87}Sr/^{86}Sr$ is 0.71138 ± 0.00014.

4.4. S–Pb isotope compositions

The $\delta^{34}S_{CDT}$ values of the Xinqiao deposit are listed in Table 6. The $\delta^{34}S_{CDT}$ values of the stratiform orebody, footwall stockwork mineralization, pyrite from pyrite-bearing quartz veins in P_1q, skarn-type deposit, and disseminated pyrite in quartz diorite range from 1.0‰ to 4.4‰ (average 2.5‰), 2.8‰ to 3.8‰ (average 3.3‰), 0.5‰ to 3.3‰ (average 2.6‰), 2.7‰ to 4.3‰ (average 3.3‰), and 2.8‰ to 4.5‰ (average 3.4‰), respectively.

The Pb isotope data of the metallic minerals and rocks from the Xinqiao deposit are listed in Table 7. The $^{208}Pb/^{204}Pb$ ratios of the stratiform orebody, footwall stockwork mineralization, pyrite from

Table 4
Hf isotope data of zircon from quartz diorite of the Jitou stock.

No.	t_{Ma}	$^{176}Yb/^{177}Hf$	$^{176}Lu/^{177}Hf$	$^{176}Hf/^{177}Hf$	2σ	$\varepsilon_{Hf}(t)$	t_{DM1}(Ma)	T_{DM2}(Ma)
3	142.5	0.041620	0.001827	0.282373	0.000014	−11.2	1269	1893
4	135.1	0.031438	0.001419	0.282378	0.000020	−11.1	1248	1884
6	137.1	0.030377	0.001352	0.282328	0.000018	−12.8	1317	1993
8	146.1	0.029214	0.001301	0.282307	0.000018	−13.4	1344	2034
9	137.2	0.043285	0.001866	0.282440	0.000023	−8.9	1175	1748
10	141.4	0.031545	0.001375	0.282433	0.000020	−9.0	1169	1758
11	141.0	0.026234	0.001172	0.282393	0.000031	−10.4	1219	1846
12	141.4	0.028401	0.001275	0.282381	0.000026	−10.8	1239	1873
13	139.2	0.034167	0.001109	0.282255	0.000664	−15.3	1410	2151
14	136.9	0.029769	0.001324	0.282388	0.000016	−10.7	1231	1860
15	138.5	0.028881	0.001334	0.282356	0.000018	−11.8	1277	1930
16	142.0	0.032498	0.001451	0.282378	0.000017	−11.0	1249	1880
17	143.7	0.030066	0.001317	0.282378	0.000028	−10.9	1245	1879
19	141.5	0.036094	0.001603	0.282447	0.000020	−8.5	1156	1729

Table 5
Rb–Sr isotope data of quartz fluid inclusions in stockwork mineralization.

Sample	Rb(ppm)	1σ	Sr(ppm)	1σ	$^{87}Rb/^{86}Sr$	$^{87}Sr/^{86}Sr$	1σ
XQ030-6-1	5.180	0.049	2.746	0.025	5.541	0.722229	0.000018
XQ030-6-2	5.151	0.051	2.723	0.024	5.556	0.722230	0.000012
XQ031-2	2.845	0.029	4.683	0.039	1.768	0.714791	0.000014
D005-1	1.250	0.019	3.606	0.035	1.009	0.713404	0.000011
D011-1	9.020	0.077	4.751	0.039	5.577	0.722375	0.000012
D011-2	8.890	0.064	5.410	0.044	4.818	0.720855	0.000013

pyrite-bearing quartz veins in the Qixia Formation, skarn-type deposit, disseminated pyrite in quartz diorite, and dolomite in Huanglong Formation are 37.879–38.556, 38.325–38.756, 38.353–38.491, 38.300–38.472, 38.272–38.386, and 38.781, respectively. Their $^{207}Pb/^{204}Pb$ ratios are 15.557–15.616, 15.541–15.577, 15.577–15.615, 15.545–15.565, 15.542–15.567, and 15.659, respectively, and their $^{206}Pb/^{204}Pb$ ratios are 18.213–18.557, 18.397–18.575, 18.279–18.564, 18.374–18.452, 18.305–18.409, and 18.317, respectively.

5. Discussion

5.1. Origin of magma

For the magmatic sources in the Tongling ore district, there are mainly two viewpoints. One point proposed that the magma is derived from the mantle with contributions from ancient crust (Xing and Xu, 1996; Tang et al., 1998; Deng and Wu, 2001), while

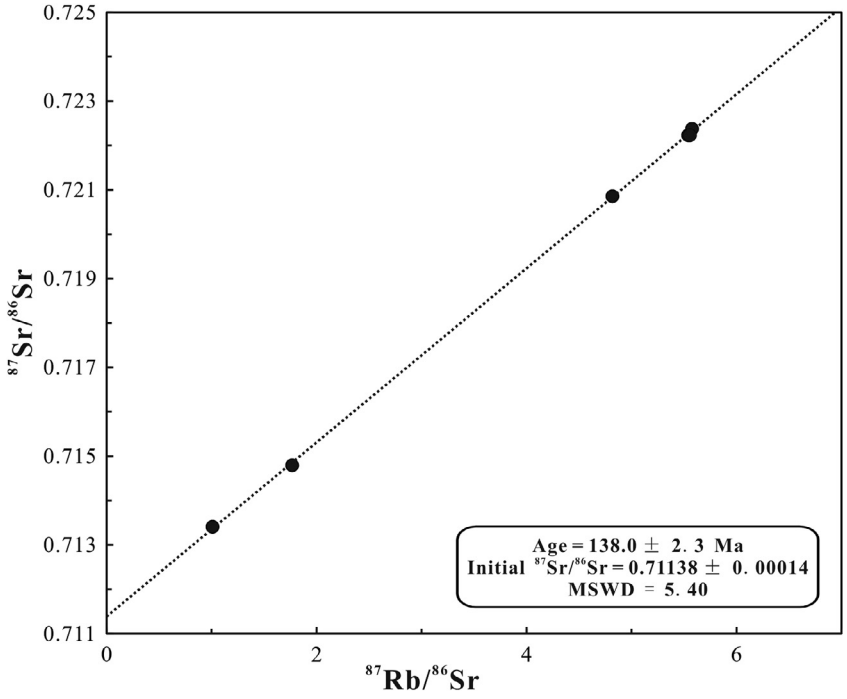

Fig. 9. Rb–Sr isotope isochron diagram of quartz fluid inclusions from the footwall stockwork mineralization.

Table 6
$\delta^{34}S_{CDT}$ values of sulfides and rocks of the Xinqiao deposit.

Sample	Description	Mineral	$\delta^{34}S_{CDT}$(‰)	Data source
D001-1	Stratiform orebody	Galena	1.7	
D001-2	Stratiform orebody	Galena	1.3	
D002	Stratiform orebody	Pyrite	3.5	
D002	Stratiform orebody	Sphalerite	2.6	
D007-6	Stratiform orebody	Pyrite	4.4	
D007-6	Stratiform orebody	Pyrrhotite	4.4	
XQ045-5	Stratiform orebody	Pyrite	1.0	
XQ045-6	Stratiform orebody	Pyrite	3.6	
XQ008	Stratiform orebody	Pyrite	3.2	
XQ047-5	Stratiform orebody	Pyrite	3.8	
XQ012	Stratiform orebody	Pyrite	3.0	
XQ011	Stratiform orebody	Pyrite	1.0	
XQ011-1	Stratiform orebody	Pyrite	1.1	
XQ011-2	Stratiform orebody	Pyrite	1.0	
D005-2	Footwall stockwork mineralization	Pyrite	2.8	
D006-2	Footwall stockwork mineralization	Pyrite	3.0	
D011-1	Footwall stockwork mineralization	Pyrite	3.2	
D011-2	Footwall stockwork mineralization	Pyrite	3.7	
XQ045-8	Footwall stockwork mineralization	Pyrite	3.8	
D010-1	Pyrite-bearing quartz veins in Qixia Formation	Pyrite	3.3	
D010-2	Pyrite-bearing quartz veins in Qixia Formation	Pyrite	4.0	
D010-3	Pyrite-bearing quartz veins in Qixia Formation	Pyrite	0.5	
D007-5a	Skarn-type orebody	Pyrite	4.3	
XQ007	Skarn-type orebody	Pyrite	2.8	
D012-1	Skarn-type orebody	Pyrite	2.7	
D013-1	Disseminated pyrite in quartz diorite	Pyrite	2.9	
D016-3	Disseminated pyrite in quartz diorite	Pyrite	2.8	
D016-4	Disseminated pyrite in quartz diorite	Pyrite	4.5	
XQ045-3	Huanglong Formation	Dolomite	−9.47 to −15.42	Tang et al., 1998

Table 7
Pb isotope ratios of metallic minerals and rocks from the Xinqiao deposit.

Sample	Description	Mineral	$^{208}Pb/^{204}Pb$	$^{207}Pb/^{204}Pb$	$^{206}Pb/^{204}Pb$	Data source
D001-1	Stratiform orebody	Galena	38.551	15.607	18.484	
D007-5b	Stratiform orebody	Magnetite	37.879	15.570	18.213	
XQ008	Stratiform orebody	Pyrite	38.380	15.571	18.398	
XQ045-6	Stratiform orebody	Pyrite	38.379	15.589	18.320	
XQ011	Stratiform orebody	Pyrite	38.427	15.584	18.372	
XQ011-1	Stratiform orebody	Pyrite	38.454	15.584	18.332	
XQ011-2	Stratiform orebody	Pyrite	38.556	15.616	18.353	
XQ045-7	Stratiform orebody	magnetite	38.281	15.557	18.557	
D010-2	Pyrite-bearing quartz veins in Qixia Formation	Pyrite	38.353	15.577	18.564	
D010-3	Pyrite-bearing quartz veins in Qixia Formation	Pyrite	38.491	15.615	18.279	
D011-1	Footwall stockwork mineralization	Pyrite	38.472	15.577	18.416	
D011-2	Footwall stockwork mineralization	Pyrite	38.325	15.541	18.397	
XQ45-8	Footwall stockwork mineralization	Pyrite	38.756	15.609	18.575	
D012-1	Skarn-type orebody	Pyrite	38.300	15.545	18.374	
XQ007	Skarn-type orebody	Pyrite	38.472	15.565	18.452	
D013-1	Disseminated pyrite in quartz diorite	Pyrite	38.272	15.542	18.409	
D016-3	Disseminated pyrite in quartz diorite	Pyrite	38.386	15.567	18.385	
XQ45-3	Huanglong Formation	Dolomite	38.781	15.659	19.317	
	Jitou stock	K-feldspar	38.244	15.488	18.421	Zang et al., 2007
	Jitou stock	K-feldspar	38.225	15.512	18.363	
	Jitou stock	K-feldspar	38.090	15.482	18.273	

the other suggested a remelted source from the lower crust for the Yangtze Block (Du and Li, 1997; Zhang et al., 2001).

Lead isotope data of K-feldspar in the quartz diorite from Jitou stock, plot near the mantle line rather than the lower or upper crust lines in $^{206}Pb/^{204}Pb$ vs. $^{207}Pb/^{204}Pb$ and $^{208}Pb/^{204}Pb$ diagrams (Fig. 10), suggesting that original magma for the Jitou stock was contributed by more or less mantle materials. The Nb/Ta average ratio of quartz diorite from Jitou stock is 14.7 (Zhang et al., 2014), lower than the average primitive mantle (17.5, Sun and McDonough, 1989) and MORB (16.7, Kamber and Collerson, 2000), but higher than the average continental crust (12.0–13.0, Barth et al., 2000), resembling crustal-derived magmas with mantle material input, as supported by the initial $^{87}Sr/^{86}Sr$ value (0.7065) of the quartz diorite, which is distinct from those of both mantle and crust values (Yu et al., 1998). Mg# is an important indicator to determine whether there is mantle-derived magma mingling and it is more than 40 for mantle material input (Rapp and Watson, 1995). We obtained Mg# of Jitou stock ranging from 30 to 47 by using the major elements compositions reported by Zhang et al. (2014), and some Mg# are more than 40, indicating that the magma for Jitou stock contain some mantle material. Zircon Hf isotope composition is also useful in determining the possible magma sources (Woodhead et al., 2001; Kemp et al., 2007). The $\varepsilon_{Hf}(t)$ of the Jitou stock have a range of −15.3 to −8.5 (Table 4 and

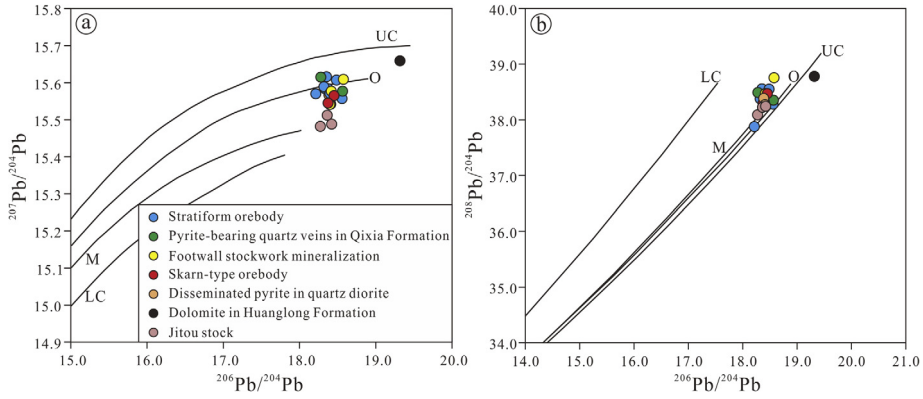

Fig. 10. (a) $^{206}Pb/^{204}Pb$ vs. $^{207}Pb/^{204}Pb$ and (b) $^{206}Pb/^{204}Pb$ vs. $^{208}Pb/^{204}Pb$ diagrams showing the Pb isotope compositions of the Xinqiao deposit. UC = Upper crust, LC = Lower crust, O = Orogen, M = Mantle.

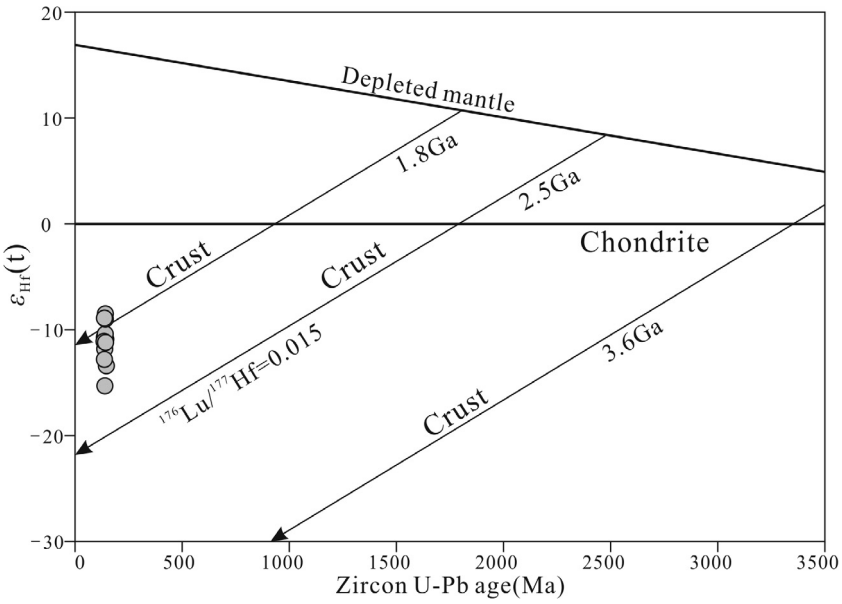

Fig. 11. Schematic diagram of the Lu–Hf isotope evolution of zircon from the Jitou quartz diorite.

Fig. 11), which indicates that the Jitou stock was mainly derived from the crust. Therefore, based on the combined information from Hf–Pb–Sr isotopes, Nb/Ta ratios and Mg#, we infer that the magma for Jitou stock probably was dominated by crustal-derived magmas with minor mantle material input.

5.2. Ore-bearing potential of the magma

As mentioned above, the average values of $\log(fO_2)$ and ΔFMQ of the magma for the Jitou stock quartz diorite can reach up to −10.85 and 4.36, respectively, with 16 among 20 ΔFMQ data being more than 2 (Fig. 12), which indicates that the Jitou quartz diorite stock was derived from the highly oxidized magma. It is widely accepted that highly oxidized magmas favor copper mineralization (Arculus, 1994; Torrence and Compo, 1998; Ballard et al., 2002; Sillitoe, 2010; Zhang et al., 2015; Lu et al., 2016). Especially, the formation of porphyry copper deposits requires high magmatic oxygen fugacity, with ΔFMQ >2 (Sun et al., 2015). Therefore, we can conclude that the highly oxidized magma for Jitou stock had a good potential to form the Cu mineralization. This conclusion is further confirmed by the Cu content in the fresh quartz diorite sample from Jitou stock which is 17 times of the Cu Clarke value (Zhang, 2015).

5.3. Source of the ore-forming material

The main metallic mineral assemblages in the stratiform orebody exhibit obvious zoning characteristics from proximal to distal: Jitou stock → magnetite + pyrite → chalcopyrite + pyrite → pyrite. Magnetite crystallizes at high temperatures and occurs closer to the Jitou stock, whereas pyrite crystallizes at low temperatures and occurs farther away from the stock. These characteristics are typical of mineral zoning in magmatic hydrothermal deposits.

The stratiform orebody, the footwall stockwork mineralization, the pyrite from pyrite-bearing quartz veins in the Lower Permian Qixia Formation, the skarn-type orebodies, and the disseminated pyrite in Jitou stock all have similar S isotope compositions and $\delta^{34}S_{CDT}$ (‰) values that lie within a relatively narrow range (0–5; Fig. 13). Most importantly, their $\delta^{34}S_{CDT}$ (‰) values are distinct from those of the dolomite in Huanglong Formation (Fig. 14), indicating that the sulfur isotopes in five types of ore were not sourced from the host rocks. Since the source of the sulfur in the skarn-type orebodies appears to be the Jitou stock, we infer that the source of the sulfur in the stratiform orebody and the footwall stockwork mineralization was also the Jitou stock.

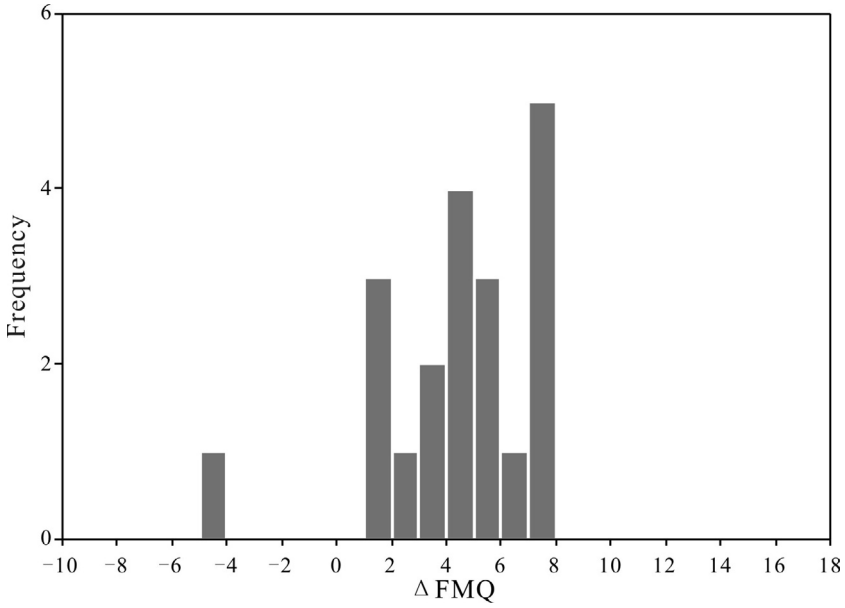

Fig. 12. ΔFMQ histogram of quartz diorite from the Jitou stock.

In $^{206}Pb/^{204}Pb$ vs. $^{207}Pb/^{204}Pb$ diagram (Fig. 10a) and $^{206}Pb/^{204}Pb$ vs. $^{208}Pb/^{204}Pb$ diagram (Fig. 10b), the Pb isotope data of five types of ores plot in a narrow area near the orogenic line, indicating that the Pb in the ores was sourced from both mantle and crust. The Pb isotope data plot very close those of the Jitou stock but far away from that of Huanglong Formation, suggesting that the ore-forming material was sourced only from the Jitou stock and not from the host rocks.

The H–O isotope data from ore-bearing quartz in the stratiform orebody show that the ore-forming fluid is dominantly a magmatic hydrothermal fluid (Liu, 2002), which is consistent with the iron isotope compostions ($\delta^{57}Fe$: −1.22‰ to 0.15‰) of pyrite in the stratiform orebody (Wang et al., 2011, 2013). Therefore, by combining the mineral zoning characteristics of the Xinqiao deposit with the S, Pb, H–O and Fe isotope data, we conclude that the stratiform orebody, the footwall stockwork mineralization and the skarn-type orebodies were genetically linked to the Yanshanian magmatic activity related to the Jitou stock.

5.4. Genesis of the footwall stockwork mineralization

The footwall stockwork mineralization of the stratiform orebody is dominated by pyrite-quartz veins (Fig. 5a, b), distinct from the mineral assemblage (such as anhydrite and barite) of typical SEDEX footwall stockwork mineralization (Sangester, 1990). More importantly, the footwall alteration of the Xinqiao stratiform orebody is dominated by the alteration of chert, inconsistent with typical SEDEX deposits, which is characterized by tourmaline, albitite, chlorite and epidote alterations (Sangester, 1990).

Although the Re–Os isochron age (319 ± 13 Ma; Guo et al., 2011) of pyrite from the footwall stockwork mineralization may imply the Late Paleozoic submarine exhalative origin for the Xinqiao deposit, the initial value of $^{187}Os/^{188}Os$ (0.017) is inconsistent with the initial $^{187}Os/^{188}Os$ of typical SEDEX deposits, which usually lie in the range between average oceanic crust (~1) and seawater (~8) (Ravizza et al., 1996), and ^{187}Os vs. ^{187}Re ratios of pyrites plot in a fairly narrow field, which do not meet the conditions of Re–Os isochron age and most likely the true age of the footwall stockwork mineralization (Huang, 2011). In this study, Rb–Sr dating of quartz fluid inclusions in the footwall stockwork mineralization yielded an age of 138.0 ± 2.3 Ma (MSWD = 5.4), close to the formation age of Jitou stock (138.4 ± 2.3 Ma, MSWD = 1.4). More importantly, the footwall stockwork mineralization yielded an initial $^{87}Sr/^{86}Sr$ of 0.71138 ± 0.00014, similar to those of the stratiform orebody (0.710; Li et al., 1997) and the Jitou stock (0.7065; Yu et al., 1998), but different from the value of the ore-hosting limestone (0.7246; Zhang, 2015), as also demonstrated by the similar S and Pb isotope compositions of the footwall stockwork mineralization (Figs. 10, 13 and 14).

Therefore, we concluded that the footwall stockwork mineralization was likely to be genetically linked to the magmatic-hydrothermal fluids associated with the Jitou stock.

5.5. Implications for ore genesis

As mentioned above, three hypotheses for the Xinqiao ore genesis were proposed, with the major controversies focusing on whether: 1) the source of the ore-forming material was from the magma for Jitou stock, and 2) the footwall stockwork mineralization was of Jurassic-Cretaceous magmatic-hydrothermal or Late Paleozoic submarine exhalative origin. The evidence outlined in the sections above has clearly supported a magmatic hydrothermal origin for the stratiform orebody and the footwall stockwork mineralization. In general, the stratiform orebody (including the footwall stockwork mineralization) and the Jitou stock are genetically related in four aspects. Firstly, there is a close spatial relationship. In the stratiform orebody, the mineralization close to Jitou stock is more enriched (Fig. 4), and the mineral assemblages in the stratiform orebody exhibit the typical mineral zoning characteristics in the magmatic hydrothermal deposits. Secondly, there is a close temporal relationship, with Rb–Sr dating of the footwall stockwork mineralization close to the zircon U–Pb dating of the Jitou stock. Thirdly, S–Pb–Sr–Fe–H–O isotope compositions show that the Xinqiao mineralization is genetically linked to the magmatic-hydrothermal fluids associated with the Jitou stock. Fourthly, the high oxygen fugacity of the Jitou stock magma is favorable for the Cu mineralization.

In addition, the parallel unconformity between Upper Devonian Wutong Formation and Upper Carboniferous Huanglong Formation, constraining the Xinqiao stratiform orebody, reveals a terrigenous setting or a shallow sea setting (Mao et al., 2009), which are inconsistent with typical SEDEX deposits that usually

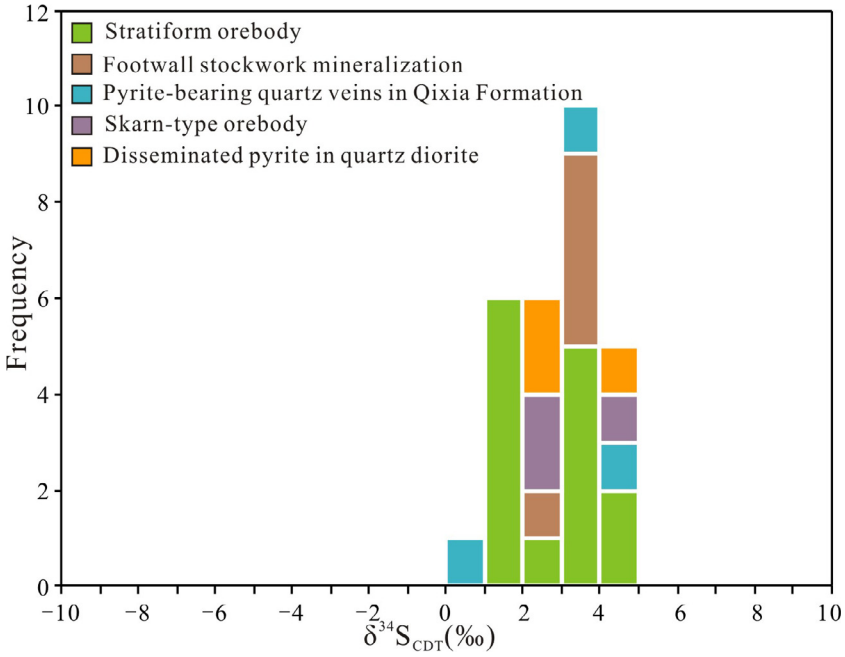

Fig. 13. Histogram of the S isotope composition of sulfides from the Xinqiao deposit.

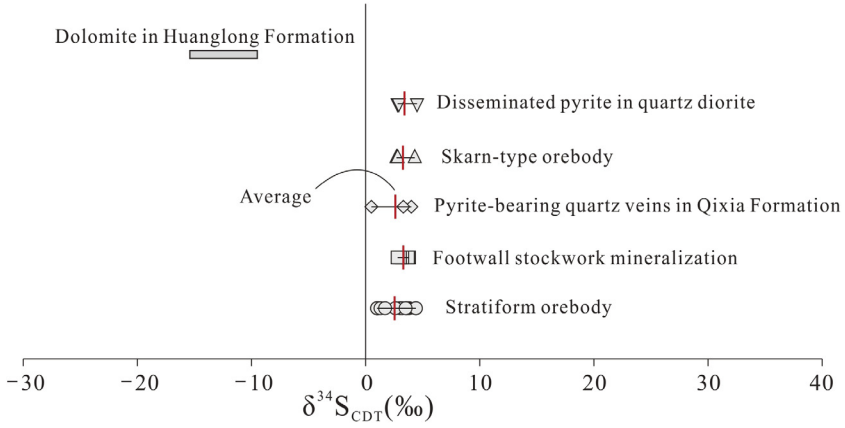

Fig. 14. $\delta^{34}S_{CDT}$ (‰) values of the Xinqiao deposit and related lithologies ($\delta^{34}S_{CDT}$ of dolomite in Huanglong Formation are from Tang et al., 1998).

form in deep sea setting (1.5–3.5 km water depth; Scott, 2008). Moreover, typical SEDEX deposits are characterized by syngenetic mineralization, but there is a clear abrupt contact interface between the Xinqiao stratiform orebody and the Wutong Formation quartz sandstone (Fig. 5c), indicative of epigenetic mineralization.

Based on the above discussion, we conclude that the stratiform orebody (including the footwall stockworks mineralization) at Xinqiao was likely to have formed from Yanshanian magmatic-hydrothermal fluids, probably associated with the nearby Jitou stock and the Xinqiao Cu–S–Fe–Au mineraization may have been generated by the Yanshanian tectono-thermal event in Eastern China.

The possible geodynamic setting and ore-forming process of the Xinqiao deposit are as follows:

From ca. 180 to 90 Ma, the continental margin of Eastern China may have evolved from an active continental margin to an intraplate setting, and the stress field may have changed from compressive to extensional (Qi et al., 2000). When the subduction of the paleo-Pacific plate began and the continental crust of the Yangtze craton delaminated, structural orientation of the Middle-Lower Yangtze River Valley metallogenic belt may have changed from E–W to NE–SW trending, and then to NNE–SSW trending (Zhou et al., 2008), and the resultant complex crustal-mantle interactions may have generated intense magmatism (Wu et al., 2003; Mao et al., 2013). Under such tectono-magmatic regime, the region between the Jitou-Shatanjiao basement fault and the NNE–SSW-trending fault zone was extended, leading to the magma from the lower crust upwelling. The magmas may have migrated along the NE-trending Dachengshan anticline and the NNE-trending Shenchong syncline to form the NW-trending Jitou stock (Liu et al., 1996). Subsequently, magmatic-hydrothermal fluids enriched in ore-forming elements (e.g., Cu, S, and Fe) may have ascended and entered the detachments between the Upper Devonian Wutong Formation quartz sandstone and the Upper Carboniferous Huanglong Formation dolomite in the Early Cretaceous (ca. 138.0 ± 2.3 Ma). This may have led to the early (Stage I) and late (Stage II) skarn alterations. With decreasing temperature, Fe in the ore-forming fluids precipitated to form hematite and magnetite (Stage III). The Fe-oxides mineralization and the fluid mixing had substantially altered the physicochemical conditions

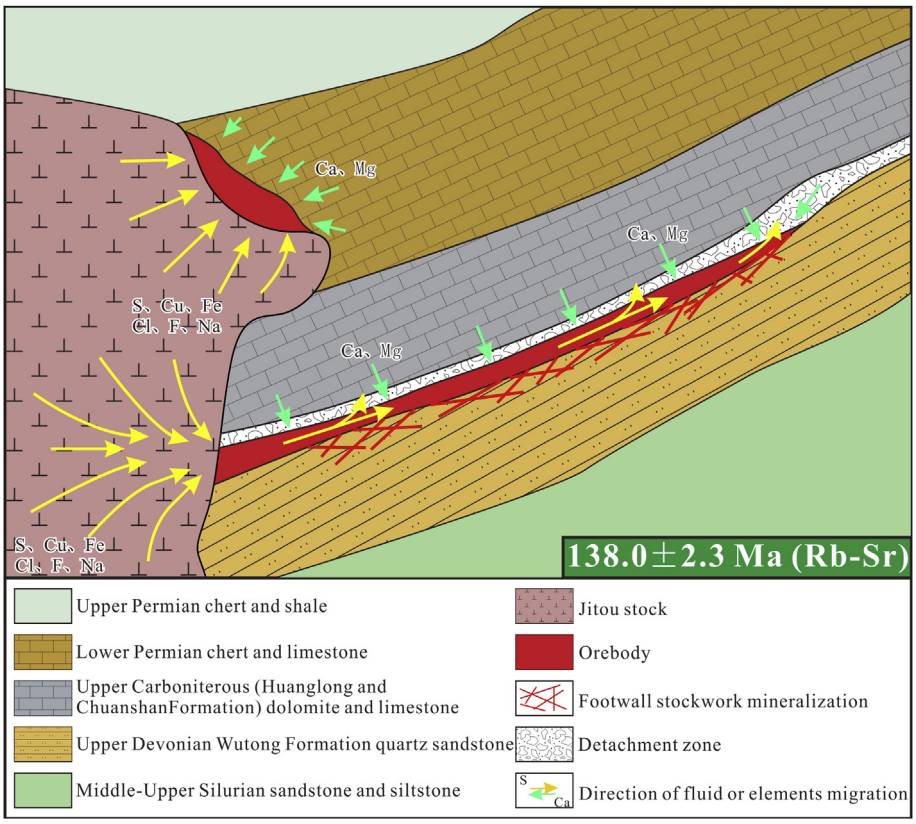

Fig. 15. Genetic model of the Xinqiao Cu–S–Fe–Au deposit.

of the ore fluids, and generated large temperature fluctuations and undercooling, resulting in the rapid crystallization of Stage IV colloform pyrites (Py1) that locally cemented the early massive magnetite (Zhang, 2015). Continuous influx of the ore-forming fluids and temperature drop may have led to the formation of abundant quartz, fine to coarse-grained pyrite and chalcopyrite with local pyrrhotite, galena, sphalerite, sericite, chlorite and calcite (Stage V) in the stratiform orebody. Coevally, some ore-forming fluids may have entered the Wutong Formation quartz sandstone to form the stockwork mineralization (Fig. 15; Zhang et al., 2016).

6. Conclusions

We performed *in situ* U–Pb–Hf and trace elements analysis of zircon from the quartz diorite in Jitou stock, Rb–Sr isotope analyses of fluid inclusions in quartz from the footwall stockwork mineralization of the Xinqiao Cu–S–Fe–Au deposit and systematic S–Pb isotope analyses of sulfides based on detailed field investigations. The results allow us to draw the following conclusions.

(1) The magma for Jitou stock probably was dominated by crustal-derived magmas with minor mantle material input in the early Cretaceous. And the magma had the relatively high oxygen fugacity and was favorable for the Cu mineralization.
(2) The ore-forming material of Xinqiao deposit was mainly derived from the Jitou stock.
(3) The footwall stockwork mineralization formed at ca. 138.0 ± 2.3 Ma and was likely to be genetically linked to the magmatic-hydrothermal fluids associated with the Jitou stock.
(4) The Xinqiao stratiform orebody may have been the result of the Yanshanian magmatic-hydrothermal fluids associated with the Jitou stock and generated by the Yanshanian tectono-thermal event in Eastern China.

Acknowledgements

This research was financially supported by the Project of Innovation-driven Plan in Central South University (2015CX008) and the Special Research Funding for the Public Benefit sponsored by MLR China (200911007-4). We especially thank Dr Xiong-jun Wang and Dr Ming-hong Zhen for assistance with the field work. We sincerely appreciate the detailed and constructive reviews and suggestions from four anonymous reviewers, which greatly improved this paper.

References

Arculus, R.J., 1994. Aspects of magma genesis in arcs. Lithos 33, 189–208.
Ballard, J.R., Michael, P., Campbell, H.I., 2002. Relative oxidation states of magmas inferred from Ce(IV)/Ce(III) in zircon: application to porphyry copper deposits of northern Chile. Contrib. Mineral. Petrol. 144, 347–364.
Barth, M.G., McDonough, W.F., Rudnick, R.L., 2000. Tracking the budget of Nb and Ta in the continental crust. Chem. Geol. 165, 197–213.
Cao, Y., Zheng, Z.J., Du, Y.L., Gao, F.P., Qin, X.L., Yang, H.M., Lu, Y.H., Du, Y.S., 2017. Ore geology and fluid inclusions of the Hucunnan deposit, Tongling, Eastern China: implications for the separation of copper and molybdenum in skarn deposits. Ore Geol. Rev. 81, 925–939.
Chang, Y.F., Liu, X.G., 1983. Layer control type skarn type deposit—some deposits in the Middle-Lower Yangtze Depression in Anhui Province as an example. Miner. Deposits 2 (1), 11–20 (in Chinese).
Chang, Y.F., Liu, X.P., Wu, Y.C., 1991. The Copper–Iron Belt of the Lower and Middle Reaches of the Changjiang River. Geological Publishing House, Beijing, p. 379 (in Chinese with English abstract).

Deng, J.F., Wu, Z.X., 2001. Lithospheric thinning event in the Lower Yangtze Craton and Cu-Fe metallogenic belt in the Middle-Lower Yangtze River reaches. Anhui Geol. 11 (2), 86–91 (in Chinese with English abstract).
Du, Y.L., Deng, J., Cao, Y., Li, D.D., 2015. Petrology and geochemistry of Silurian-Triassic sedimentary rocks in the Tongling region of Eastern China: their roles in the genesis of large stratabound skarn ore deposits. Ore Geol. Rev. 67, 255–263.
Du, Y.S., Li, X.J., 1997. Enclaves in the typical mining districts of Tongling, Anhui and their implication to the process of magmatism-metallogeny. Geol. J. China Univ. 3 (2), 17l–182 (in Chinese with English abstract).
Fu, S.G., Yan, X.Y., Yuan, C.X., 1977. Geologic feature of submarine volcanic eruption-sedimentary pyrite type deposit in Carboniferous in the Middle-Lower Yangtze River Valley metallogenic belt, Eastern China. J. Nanjing Univ. (Nat. Sci.) 4, 43–67 (in Chinese).
Gu, L.X., Hu, W.X., He, J.X., 2000. Regional variations in ore composition and fluid features of massive sulfide deposits in South China: implications for genetic modeling. Episodes 23 (2), 110–118.
Guo, W.M., Lu, J.J., Jiang, S.Y., Zhang, R.Q., Qi, L., 2011. Re-Os isotope dating of pyrite from the footwall mineralization zone of the Xinqiao deposit, Tongling, Anhui Province: geochronological evidence for submarine exhalative sedimentation. Chinese Sci. Bull. 56 (36), 3860–3865 (in Chinese with English abstract).
Hu, Z.C., Liu, Y.S., Gao, S., Liu, W.G., Yang, L., Zhang, W., Tong, X., Lin, L., Zong, K.Q., Li, M., Chen, H.H., Zhou, L.A., Yang, L., 2012. Improved in situ Hf isotope ratio analysis of zircon using newly designed X skimmer cone and Jet sample cone in combination with the addition of nitrogen by laser ablation multiple collector ICP-MS. J. Anal. At. Spectrom. 27, 1391–1399.
Huang, G.H., 2011. Mineralization characteristics and genesis of Xinqiao Cu-S-Au polymetallic deposit, Tongling, Anhui Province, China (Master Thesis). China University of Geosciences, Wuhan (in Chinese with English abstract).
Kamber, B.S., Collerson, K.D., 2000. Role of 'hidden' deeply subducted slabs in mantle depletion. Chem. Geol. 166, 241–254.
Kemp, A.I.S., Hawkesworth, C.J., Foster, G.L., Paterson, B.A., Woodhead, J.D., Hergt, J. M., Gray, C.M., Whitehouse, M.J., 2007. Magmatic and crustal differentiation history of granitic rocks from hafnium and oxygen isotopes in zircon. Science 315, 980–983.
Lai, J.Q., Chi, G.X., 2007. CO_2-rich fluid inclusions with chalcopyrite daughter mineral from the Fenghuangshan Cu–Fe–Au deposit, China: implications for metal transport in vapor. Miner. Deposita 42, 293–299.
Li, W.D., Wang, W.B., Fang, H.Y., 1997. Ore-forming conditions of Cu (Au) deposit-intensive areas and existence possibility of super large ore deposit in the Middle-Lower Yangtze River Valley metallogenic belt. Volcanol. Miner. Res. 20 (s), 1–131.
Li, S., Yang, X.Y., Huang, Y., Sun, W.D., 2014. Petrogenesis and mineralization of the Fenghuangshan skarn Cu–Au deposit, Tongling ore cluster field, Lower Yangtze metallogenic belt. Ore Geol. Rev. 58, 148–162.
Ling, M.X., Wang, F.Y., Ding, X., Hu, Y.H., Zhou, J.B., Zartman, R.E., Yang, X.Y., 2009. Cretaceous rifge subduction along the Lower Yangtze River Belt, Eastern China. Econ. Geol. 104, 303–321.
Liu, X.B., 2002. Geological characteristics and ore-controlling factor analysis of Xinqiao S-Fe deposit. Express Inf. Min. Ind. 22, 13–15 (in Chinese).
Liu, W.C., Gao, D.Z., Chu, G.Z., 1996. Aanalysis of tectonic deformation and metallogenic prediction in Tongling region. Geological Publishing House, Beijing, pp. 1–131 (in Chinese).
Liu, Y.S., Gao, S., Hu, Z.C., Gao, C.G., Zong, K.Q., Wang, D.B., 2010. Continental and oceanic crust recycling-induced melt-peridotite interactions in the Trans-North China Orogen: U-Pb dating, Hf isotopes and trace elements in zircon of mantle xenoliths. J. Petrol. 51, 537–571.
Lu, Y.J., Loucks, R.R., Fiorentini, M., McCuaig, C., Evans, N.J., Yang, Z.M., Hou, Z.Q., Kirkland, C.L., Parra-Avila, L.A., Kobussen, A., 2016. Zircon Compositions as a Pathfinder for Porphyry Cu ± Mo ± Au Deposits. Econ. Geol. 19, 329–347.
Ludwig, K.R., 2012. User's Manual for Isoplot 3.75: A Geochronological Toolkit for Microsoft Excel. Berkeley Geochronology Center, Berkeley, pp. 1–70.
Mao, J.W., Wang, Y.T., Lehmann, B., Yu, J.J., Du, A.D., Mei, Y.X., Li, Y.F., Zang, W.S., Stein, H.J., Zhou, T.F., 2006. Molybdenite Re–Os and albite $^{40}Ar/^{39}Ar$ dating of Cu-Au-Mo and magnetite porphyry systems in the Changjiang valley and metallogenic implications. Ore Geol. Rev. 29, 307–324.
Mao, J.W., Shao, Y.J., Xie, G.Q., Zhang, J.D., Chen, Y.C., 2009. Mineral deposit model for porphyry-skarn polymetallic copper deposits in Tongling ore dense district of Middle-Lower Yangtze Valley metallogenic belt. Miner. Deposits 28 (2), 109–119 (in Chinese with English abstract).
Mao, J.W., Xie, G.Q., Duan, C., Franco, P., Dazio, I., Chen, Y.C., 2011. A tectono-genetic model for porphyry-Skarn-Stratabound Cu-Au-Fe and magnetite-apatite deposit along the Middle-Lower Yangtze River Valley, Eastern China. Ore Geol. Rev. 43 (1), 294–314.
Mao, J.W., Cheng, Y.B., Chen, M.H., Pirajno, F., 2013. Major types and time-space distribution of Mesozoic ore deposits in South China and their geodynamic settings. Miner. Deposits 48, 267–294.
Meng, L.Y., 1994. Invasive type massive sulfide deposits in the Eastern China. Sci. China Ser. D 24 (1), 76–80 (in Chinese).
Meng, L.Y., 1996. Stable isotopes compositions characteristics of invasive type massive sulfide deposits. Chinese Sci. Bull. 41 (9), 808–810 (in Chinese).
Pan, Y., Done, P., 1999. The lower Changjiang (Yangtzi/Yangtze River) metallogenic belt, east-center China: intrusion and wall rock hosted Cu-Fe-Au, Mo, Zn, Pb, Ag deposits. Ore Geol. Rev. 15 (4), 177–242.
Qi, J.Z., Liu, H.Y., Jiang, Y.H., 2000. Yanshanian subduction and strike-sliping regime of East China, and its control of ore localization. Volcanol. Miner. Resour. 21 (4), 244–266 (in Chinese with English abstract).
Rapp, R.P., Watson, E.B., 1995. Dehydration melting of metabasalt at 8–32 kbar: implications for continental growth and crust-mantle recycling. J. Petrol. 36 (4), 891–931.
Ravizza, G., Martin, C.E., German, C.R., Thompson, G., 1996. Os isotopes as tracers in seafloor hydrothermal system: metalliferous deposits from the TAG hydrothermal area, 26°N Mid-Atlantic Ridge. Earth Plant. Sci. Lett. 138, 105–119.
Rossman, G.R., Weis, D., Wasserburg, G.J., 1987. Rb, Sr, Nd and Sm concentrations in quartz. Geochmi. Cosmochmi. Acta 51, 2325–2329.
Sangester, D.F., 1990. Mississippi Valley-type and SEDEX lead-zinc deposits—a comparative examination. Inst. Min. Metall. Trans., Sect. B, Appl. Earth Sci. 99, 21–42.
Scott, S.D., 2008. Massive sulfide deposits on the deep ocean floor-The dawning of a new mining history. In: Pacific rim: Mineral endowment, discovery & exploration frontiers. The Australasian Institute of Mining and Metallurgy, pp. 19–22.
Sillitoe, R.H., 2010. Porphyry copper systems. Econ. Geol. 105, 3–41.
Sun, S.S., McDonough, W.F., 1989. Chemical and isotopic systematics of ocean basalts: implications for mantle composition and process. In: Saunders, A.D., Norry, M.J. (Eds.), Magmatism in the Ocean Basins. Geological Society, London, Special Publications, pp. 313–345.
Sun, W.D., Huang, R.F., Li, H., Hu, Y.B., Zhang, C.C., Sun, S.J., Zhang, L.P., Ding, X., Li, C. Y., Zartman, R.E., Ling, M.X., 2015. Porphyry deposits and oxidized magmas. Ore Geol. Rev. 65, 97–131.
Tang, Y.C., Wu, Y.Z., Cu, G.Z., Xing, F.M., Wang, Y.M., Cao, F.Y., Chang, Y.F., 1998. Copper gold polymetallic ore deposit geology in the region along Yangtze River in Anhui Province. Geological Publishing House, Beijing, pp. 1–351 (in Chinese).
Torrence, C., Compo, G.P., 1998. A practical guide to wavelet analysis. Bull. Am. Meteorol. Soc. 79 (1), 61–78.
Trail, D., Watson, E.B., Tailby, N.D., 2011. The oxidation state of Hadean magmas and implications for early Earth's atmosphere. Nature 480, 79–82.
Wang, Y.B., Liu, D.Y., Meng, Y.F., Zeng, P.S., Yang, Z.S., Tian, S.A., 2004. SHRIMP U-Pb geochronology of the Xinqiao Cu-S-Fe-Au deposit in the Tongling ore district, Anhui, China. Geol. China 31 (2), 169–173 (in Chinese with English abstract).
Wang, Y.X., Yang, J.D., Chen, J., Zhang, K.J., Rao, W.B., 2007. The Sr and Nd isotopic variations of the Chinese Loess Plateau during the past 7 Ma: implications for the East Asian winter monsoon and source areas of loess. Palaeogeogr. Palaeoclimatol. Palaeoecol. 249, 351–361.
Wang, Y., Zhu, X.L., Mao, J.W., Li, Z.H., Cheng, Y.B., 2011. Iron isotope fractionation during skarn-type metallogeny: a case study of Xiao Cu-S-Fe-Au deposit in the Middle-Lower Yangtze Valley. Ore. Geol. Rev. 43, 194–202.
Wang, Y., Zhu, X.K., Cheng, Y.B., 2013. Ore microscopy & Fe isotope of the Xinqiao deposit and their constraints on the ore genesis. J. Jilin Univ.: Earth Sci. Ed. 43 (6), 1787–1798 (in Chinese with English abstract).
Wang, S.W., Zhou, T.F., Yuan, F., Fan, Y., Zhang, L.J., Song, Y.L., 2015. Petrogenesis of Dongguashan skarn-porphyry Cu-Au deposit related intrusion in the Tongling district, eastern China: geochronological, mineralogical, geochemical and Hf isotopic evidence. Ore Geol. Rev. 64, 53–70.
Wang, Y.H., Zhang, F.F., Liu, J.J., Que, C.Y., 2016. Genesis of the Fuxing porphyry Cu deposit in Eastern Tianshan, China: evidence from fluid inclusions and C-H-O-S-Pb isotope systematics. Ore Geol. Rev. 79, 46–61.
Watson, E.B., Wark, D.A., Thomas, J.B., 2006. Crystallization thermometers for zircon and rutile. Contrib. Miner. Petrol. 151, 413–433.
Woodhead, J.D., Hergt, J.M., Davidson, J.P., Eggins, S.M., 2001. Hafnium isotope evidence for 'conservative' element mobility during subduction zone processes. Earth. Planet. Sci. Lett. 192, 331–346.
Wu, F.Y., Ge, W.C., Sun, D.Y., Guo, C.L., 2003. Discussions on the lithospheric thinning in Eastern China. Earth Sci. Front. 10 (3), 51–60 (in Chinese with English abstract).
Wu, Y.B., Zheng, Y.F., Zhang, S.B., 2007. Zircon U-Pb ages and Hf isotope compositions of migmatite from the North Dabie terrane in China: constrains on partial melting. J. Metamorph. Geol. 25 (9), 991–1009.
Wu, C.L., Dong, S.W., Robinson, P.T., Frost, B.R., Gao, Y.H., Lei, M., Chen, Q.L., Qin, H.P., 2014. Petrogenesis of high-K, calc-alkaline and shoshonitic intrusive rocks in the Tongling area, Anhui Province (eastern China), and their tectonic implications. Geol. Soc. Am. Bull. 126, 78–102.
Xiao, X.J., Ni, P., 2000. Discussion of comparison of metallogeny for Sedex and sedimentary-rework base metal deposit. Geol. Prospect. Rev. 15 (3), 238–245 (in Chinese with English abstract).
Xie, J., 2012. Study on the pyrite and the implications for genesis of Xinqiao deposit, Anhui Province, China (Master Thesis). Hefei University of Technology, Hefei (in Chinese with English abstract).
Xie, H.G., Wang, W.B., Li, W.D., 1995. The gensis and metallogenetic of Xinqiao Cu-S Deposit, Anhui Province. Volcanol. Miner. Resour. 16 (2), 101–107 (in Chinese with English abstract).
Xie, J.C., Yang, X.Y., Du, J.G., Du, X.W., Xiao, Y.L., Qu, W.J., Sun, W.D., 2009. Re-Os precise dating of pyrite from the Xinqiao Cu-Au-Fe-S Deposit in Tongling, Anhui and its implications for minerlization. Geol. Sci. 44 (1), 183–192 (in Chinese with English abstract).
Xing, F.M., Xu, Y., 1996. High potassium calcium alkaline intrusive rocks in Tongling, Anhui Province. Geochemistry 25 (1), 29–38 (in Chinese with English abstract).
Xu, G., Zhou, J., 2001. The Xinqiao Cu-S-Fe-Au deposit in the Tongling mineral district, China: synorogenetic remobilization of a stratiform sulfide deposit. Ore Geol. Rev. 18, 77–94.
Xu, W.Y., Yang, Z.S., Meng, Y.F., Zeng, P.S., Shi, D.N., Tian, S.H., Li, H.Y., 2004. Genetic model and dynamic migration of ore-forming fluids in carboniferous

exhalation-sedimentary massive sulfide deposits in Tongling District, Anhui Province. Miner. Deposits 23 (3), 353–364 (in Chinese with English abstract).
Yang, D.F., Fu, D.X., Wu, N.X., 1982. Genesis of pyrite type copper in Xinqiao and its neighboring region according to ore composition and structure. Issue Nanjing Inst. Geol. Miner. Resour., Chinese Acad. Geol. Sci. 3 (4), 59–68 (in Chinese with English abstract).
Yu, C.W., Cen, K., Bao, Z.Y., 1998. Dynamics of mineralization. Geological Publishing House, Beijing, pp. 1–224 (in Chinese).
Zang, W.S., Wu, G.G., Zhang, D., Liu, A.H., 2004. Geological and geochemical characteristics and genetic analyses of Xinqiao Iron Orefield, Tongling. Geotec. Metall. 28 (2), 187–193 (in Chinese with English abstract).
Zang, W.S., Wu, G.G., Zhang, D., Zhang, X.X., Li, J.W., Liu, A.H., Zhang, Z.Y., 2007. A preliminary discussion on genesis of Xinqiao S-Fe orefield. Miner. Deposits 26 (4), 464–474 (in Chinese with English abstract).
Zhai, Y.S., Yao, S.Z., Lin, X.D., Jin, F.Q., Zhou, X.R., Wan, T.F., Zhou, Z.G., 1992. Metallogenic regularity of iron and copper deposits in the Middle-Lower valley of the Yangtze River. Miner. Deposits 11 (1), 1–235 (in Chinese with English abstract).
Zhang, Y., 2015. Genesis of Xinqiao Cu-S-Fe-Au deposit, Tongling, Anhui Province, China (PhD Thesis). Central South University, Changsha (in Chinese with English abstract).
Zhang, Q., Zhao, T.P., Qian, Q., Wang, Y.L., Yang, J.H., Yu, Y., 2001. A Discussion on the Yanshanian Magmatism in Eastern China. Acta Petrol. Mineral. 20, 273–280 (in Chinese with English abstract).
Zhang, Y., Shao, Y.J., Liu, Z.F., Peng, N.H., Zheng, M.H., 2014. Geological ore-formation conditions and genesis of Xinqiao Cu-S-Fe-Au deposit, Tongling, Anhui Province, China. J. Central South Univ. (Sci. Technol.) 45 (10), 3189–3498 (in Chinese with English abstract).
Zhang, D.Y., Zhou, T.F., Yuan, F., Xiao, W.J., White, N.C., Deng, Y.F., Lu, W.W., Deng, G., 2015. Petrogenesis and mineralization potential of a granite porphyry intrusion beneath the Baishan Mo deposit, Eastern Tianshan, NW China. J. Asian Earth Sci. 113, 254–265.
Zhang, Y., Shao, Y.J., Chen, H.Y., Liu, Z.F., Li, D.F., 2016. A hydrothermal origin for the large Xinqiao Cu-S-Fe deposit, Eastern China: evidence from sulfide geochemistry and sulfur isotopes. Ore Geol. Rev. http://dx.doi.org/10.1016/j.oregeorev.2016.08.002.
Zhao, Z.H., 2010. Trace element geochemistry of accessory minerals and its applications in petrogenesis and metallogenesis. Earth Sci. Front. 17 (1), 267–286.
Zhou, T.F., Yue, S.C., 2000. Ore-forming fluid system formation conditions and mechanism of Two series of copper gold deposit in the middle and lower reaches of Yangtze River. J. Peking Univ. (Nat. Sci. Ed.) 36 (5), 697–707 (in Chinese with English abstract).
Zhou, T.F., Zhang, L.J., Yuan, F., Fang, Y., Cooke, D.R., 2010. LA-ICP-MS in situ trace element analysis of pyrite from the Xinqiao Cu-Au-S Deposit in Tongling, Anhui, and its constrains on the ore genesis. Earth Sci. Front. 17 (2), 306–319 (in Chinese with English abstract).